Disentangling the spatially combined and temporally lagged influences of climate oscillations on seasonal droughts in the East Asian monsoon influenced Poyang Lake Basin

Zikang Xing [a,b,c,d], Jianhui Wei [d,*], Yunliang Li [a,b,*], Xuejun Zhang [e], Miaomiao Ma [e], Peng Yi [c], Qin Ju [c], Patrick Laux [d,f], Harald Kunstmann [d,f,g]

[a] *Key Laboratory of Lake and Watershed Science for Water Security, Nanjing Institute of Geography and Limnology, Chinese Academy of Sciences, Nanjing 210008, China*
[b] *Poyang Lake Research Station for Wetland Ecosystem, Nanjing Institute of Geography and Limnology, Chinese Academy of Sciences, Jiujiang 332800, China*
[c] *The National Key Laboratory of Water Disaster Prevention, Hohai University, Nanjing 210098, China*
[d] *Institute of Meteorology and Climate Research (IMKIFU), Karlsruhe Institute of Technology, Campus Alpin, Garmisch-Partenkirchen 82467, Germany*
[e] *Research Center on Flood and Drought Disaster Reduction of the Ministry of Water Resources, China Institute of Water Resources and Hydropower Research, Beijing 100038, China*
[f] *Institute of Geography, University of Augsburg, Augsburg 86159, Germany*
[g] *Centre for Climate Resilience, University of Augsburg, Augsburg 86159, Germany*

ARTICLE INFO

ABSTRACT

Large-scale climate oscillations are the main forcings affecting regional meteorological droughts and being relevant to sources of their predictability. However, the physical mechanism of atmospheric teleconnections with respect to regional droughts is still not fully understood. In this study, a univariate-to-multivariate analysis framework is proposed to disentangle the spatially combined and temporally lagged effects of multiple oceanic-atmospheric oscillations on meteorological droughts at regional scale. Our study focuses on the largest fresh-water lake basin of China, the Poyang Lake basin (PLB). Pearson's correlation coefficient and cross-wavelet transform are used to analyze the pair-wise linear and non-linear correlations between droughts and each climate oscillation. Random forests model is used to reveal the combined influences of multiple climate oscillations. The associated atmospheric mechanism for the identified combination of climate indices with changing lags is explored by performing composite analysis. Regarding the spatially combined influences, the concurrence of El Niño-Southern Oscillation (ENSO) and North Atlantic Oscillation (NAO) are the most important drought precursors. Regarding the temporally lagged influences, ENSO with lag of 11 months and NAO with lag of 2–3 months trigger meteorological droughts. The combined effect of preceding winter El Niño and late-summer negative NAO is the primary cause for triggering autumn droughts. The positive Eurasian teleconnection pattern, triggered by ENSO and NAO and favorable for anomalous northerly currents, is the main drought-prone circulation pattern for the PLB. These findings contribute to improved understanding of joint effects of lagged teleconnections for meteorological droughts, which could eventually lead to more skillful seasonal drought forecasting.

1. Introduction

Anthropogenic climate change and intensification of human activities have already been affecting regional hydrometeorological and hydrodynamic extremes at an unprecedented rate, such as droughts and floods (Di Baldassarre et al., 2016; Skea et al., 2014; Veldkamp et al., 2015). By now, it is well accepted that extreme events are modulated and driven by complex ocean-atmosphere-land interactions across multiple spatial and temporal scales (Dai, 2011; Wood et al., 2015; Zscheischler et al., 2020). Knowledge of the role of multiple drivers and

modulators in the occurrence of extreme events across scales can contribute to improving the predictability of extreme events (Fung et al., 2020; Hao et al., 2018; Li et al., 2018; Su et al., 2005). This is particularly relevant for droughts, as the causes (i.e., modulators and drivers) of drought occurrences are extremely complex. Moreover, it has been reported that during the recent two decades droughts have occurred even in humid regions worldwide (Berg and Sheffield, 2018; Dai, 2011; Mishra and Singh, 2010). Therefore, it is important to improve our understanding by disentangling the spatially combined and temporally lagged influences of multiple large-scale climate oscillations on regional droughts, with the aim of improving drought predictability.

Numerous studies have analyzed the driving effects of climate oscillations on regional droughts. It is found that, among the multiple drivers modulators, sea surface temperatures (SSTs) and atmospheric oscillations are proven to be highly relevant for droughts (Hao et al., 2018). Specifically, anomalies in SSTs do strongly modulate variations of drought occurrence through different patterns of teleconnections (Jiang et al., 2019; Kim et al., 2017; Liu et al., 2018a; Sehgal and Sridhar, 2018; Zhang et al., 2020b). For example, SST anomalies (SSTA) in the tropical Pacific Ocean, i.e., EI Niño-Southern Oscillation (ENSO), has been recognized as one of the dominated drivers of climate extremes in different regions across the globe (Hao et al., 2018; Hermanson et al., 2017; Sordo et al., 2008). On the other hand, recent studies have indicated that the ENSO teleconnections are non-stationary likely due to modulations of additional climate oscillations (Jiang et al., 2019; Nguyen et al., 2021). For example, droughts in semi-arid Northwest Iran are strongly modulated by the combined effects of Southern Oscillation Index (SOI) and North Atlantic Oscillation (NAO) (Marj and Meijerink, 2011). Winter droughts in arid Northwestern China have occurred as a result of the combined effects of a strong negative phase of the Arctic Oscillation (AO) and a La Niña (Liu et al., 2018b). Recent studies dealing with long-term, historical rainfall records in (sub)tropical regions, e.g., southern Florida and the Everglades, indicate that ENSO has influences on the regional droughts there at short temporal scales, whereas, Pacific Decadal Oscillation (PDO) and Atlantic Multi-decadal Oscillation (AMO) have influences at longer temporal scales (Abiy et al., 2019). Therefore, it is proven that single ENSO anomalies cannot fully explain drought occurrences, and spatially combined, nonlinear effects of multiple climate oscillations need to be taken into account in terms of increasing drought predictability (Shi et al., 2017).

In addition to the above-mentioned spatially combined effects, different climate oscillations can have impacts on regional climate extremes at different temporal scales, so-called the temporally lagged influences here (Feng et al., 2020; Vicente-Serrano et al., 2011; Zhang et al., 2020a). This is due to the dynamic propagation processes from anomalies of SSTs or atmospheric circulations to regional precipitation (Vicente-Serrano et al., 2011). Accordingly, time lags are often used to quantitatively describe delays in the response of regional climatic conditions to large-scale teleconnection patterns. Studies in this direction have revealed that the impacts of El Niño on regional droughts are still detectable more than one year after its onset, such as in East Asia (Zhang et al., 2014), Euro-Mediterranean (Mariotti et al., 2002), southern Africa (Gore et al., 2020), and equatorial South America and southern North America (Pieper et al., 2021). Such lagged impacts of ENSO on droughts are particularly pronounced in regions strongly influenced by monsoon, e.g., South China (Gao et al., 2017; Xing et al., 2022): it is found that droughts in the Xijiang River basin respond to ENSO with a lag of 5–9 months (Lin et al., 2017) and droughts in the Jinjiang River basin are associated with ENSO at an unequal lag of 1.4–1.8 months (Wu et al., 2020). Therefore, studies have indicated that by taking such temporally lagged influences of multiple climate oscillations into account might increase regional drought predictability (Chen et al., 2019; Kim et al., 2017). However, the non-linearity of sea-air-land interactions makes global climate system highly complex (Mariotti et al., 2002; Zhang et al., 2020b). Hence, there is still a lack of adequate methods to identify key modulators and/or drivers of regional climate extremes (here droughts)

out of multiple spatially combined and temporally lagged large-scale climate oscillations signals.

Often, observation-driven analyses using different statistical methods are frequently applied to examine the relationship between large-scale climate oscillations and droughts in different continental regions (Shi et al., 2017). For instance, (Forootan et al., 2019) applied canonical correlation analysis to investigate the relationship between global hydrological droughts and climate indices, and regions where droughts and teleconnections are strongly interrelated have been inferred as well. In contrast to using single statistical indices, (Sehgal and Sridhar, 2018) employed four statistical methods, i.e., Pearson's correlation coefficient, coefficient of determination, index of relative co-occurrence (IOC-r), and Fisher's exact test, for an assessment of large-scale teleconnections on the watershed-scale drought in the southeastern United States. In order to tackle the non-stationary issue, cross-wavelet transform is commonly used to quantify the relations in the domain of time window and frequency, e.g., the links between groundwater drought over North China Plain and climate patterns (Wang et al., 2020a, 2020b). Moreover, probabilistic analysis of algorithms, for instance, Copula, is applied for characterize the interplay among multiple climate patterns and their linkages with precipitation (Shi et al., 2017). The above-cited studies across different climatic zones on one hand have provided evidence for the correlations between climate oscillations and droughts of different categories (Haile et al., 2020; Mishra and Singh, 2011), but on the other hand, fall short in the identification of both the spatial interactions of multiple climate oscillations and their associated, temporally lagged influences on climate extremes.

Therefore, our study targets at enhancing the understanding of the spatially combined effects of multiple oceanic-atmospheric oscillations with changing time lags on regional droughts. The research questions addressed in this study are (1) how to disentangle the spatially combined and temporally lagged effects of multiple large-scale climate modes on seasonal meteorological droughts over the basin of Poyang Lake, i.e., the largest freshwater lake in China? (2) What are the associated atmospheric mechanisms for the lagged influences of combined climate modes on seasonal droughts at regional scale? To this end, a consolidated univariate-to-multivariate analysis framework is proposed in order to quantify both pair-wise and multiple combined correlations: in this study, Pearson's correlation coefficient (Da Silva et al., 2016) and cross-wavelet transform (Grinsted et al., 2004) are employed to perform a conventional pair-wise correlation analysis. Furthermore, a machine learning algorithm, i.e., random forests is used to perform multivariate correlation analysis (Breiman, 2001). Such a framework allows to bridge multiple climate indices (with different time lags) and droughts under a hypothetical forecasting framework with different lead times. Hence, the novelty of this study lies in (1) the development of a novel framework that integrates univariate and multivariate analyses to disentangle the impacts of multiple oceanic-atmospheric oscillations on regional meteorological droughts, and (2) the focus on disentangling the spatially combined and temporally lagged teleconnections that significantly influence autumn droughts in the Poyang Lake Basin.

The spatially combined and temporally lagged influences of climate oscillations is analyzed exemplarily on droughts of the Poyang Lake basin (PLB) (see Fig. 1), where the largest freshwater lake of China is located. Our selection here is motivated by the following facts: (1) The climate and weather extremes in the PLB particularly precipitation variations and its associated disasters, here, droughts, are strongly influenced by large-scale climate oscillations, e.g., ENSO, NAO, and Indian Ocean Dipole (IOD) (Shao et al., 2016; Xiao, 2020; Zhang et al., 2014; Zhu et al., 2020a). It is found that the negative monthly precipitation anomalies (droughts) coincide with ENSO events (Guo et al., 2020) and the meteorological droughts are associated with NAO and AO especially after the early 2000s (Liu et al., 2020). (2) There are still gaps in knowledge about lagged influences of multiple climate oscillations and the potential drought precursors for the PLB, as previous studies are
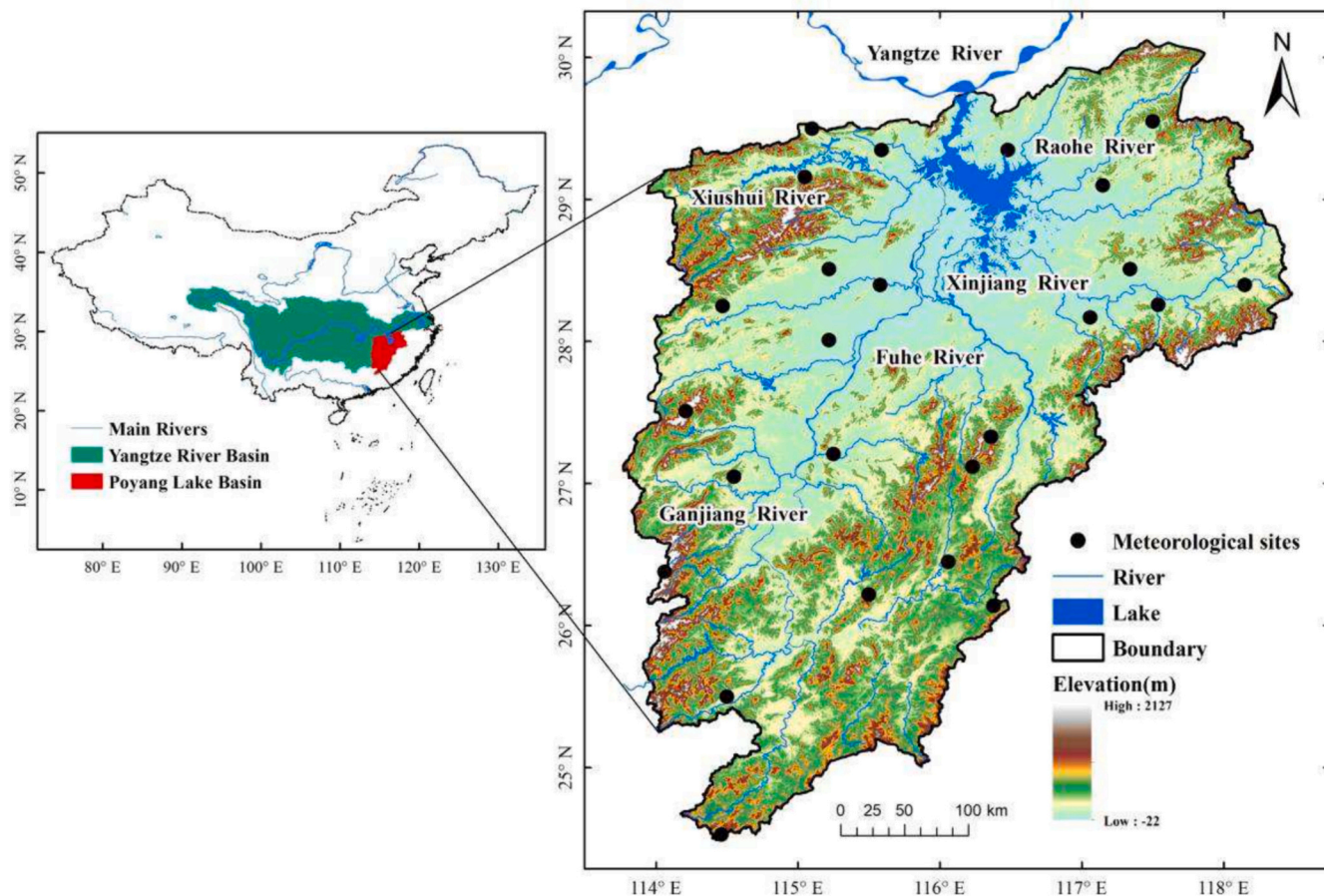
Fig. 1. Terrain height (m) of the Poyang Lake basin and spatial distribution of the meteorological stations in the basin (black circles). River networks and lakes are depicted in blue. (For interpretation of the references to color in this figure legend, the reader is referred to the web version of this article.)

limited to analyses of synchronous teleconnections between droughts and climate indices (Liu et al., 2020; Zhang et al., 2019a). (3) It is reported that in 2022 the onset of dry season for the PLB is around 16 days ahead that the recorded earliest onset (in 2006) and the associated severe seasonal drought, i.e., frequently happening during the dry season, has negative impacts on the regional water security and ecological safety (Meihan, 2022). Therefore, it is necessary to further improve our understandings of plausible physical mechanisms of droughts over the PLB from the perspectives of spatially combined and temporally lagged atmospheric circulations in order to achieve an increased leading time for predicting the droughts.

The objectives of this study are (1) to diagnose the pair-wise correlation between meteorological droughts and individual climate indices with changed lags by performing lagged correlation analysis and cross-wavelet analysis, (2) to further identify the combined effects of multiple lagged climate indices by training a random forests model, and (3) to explore the plausible atmospheric mechanism for the combined and lagged influences of the identified climate indices. The proposed framework and subsequent findings could eventually lead to improved understandings of joint effects of lagged teleconnections in terms of more skillful seasonal drought forecasting.

2. Material and methodology

2.1. Study area

Our regional drought analysis focuses on the Poyang Lake basin (PLB) in southeastern China, where the largest freshwater lake (namely, Poyang Lake) of the country is located (Wei et al., 2021). This lake

receives water from inlets of five tributaries (Xiushui, Ganjiang, Xinjiang, Fuhe, and Raohe) with a drainage area of 162,255 km^2, and has one stream outlet to the Yangtze River (Wei et al., 2015, 2016) (Fig. 1). The climate of the basin (mean precipitation ~1700 mm year^{-1}, mean annual temperature ~ 18 °C) is subtropical humid climate and is dominantly modulated by the East Asian monsoon and South Asian monsoon. Due to the fact that the rainy season in the PLB lasts only from April to June (Zhang et al., 2017), the rain-fed agriculture and the water-dependent ecosystem there are therefore highly vulnerable to climate variability-induced hydro-meteorological droughts (Hong et al., 2014). Specifically, the recently intensified droughts in the PLB, such as the severe droughts in 2003 (September to October), 2006 (July to December), 2009 (July to September), and 2019 (July to October), have leaded to a decreased agricultural productivity and economic development (Hong et al., 2014; Liu et al., 2011; Zhang et al., 2011).

2.2. Data sources

Data used in this study consists of station-based meteorological records, climate indices, and gridded atmospheric reanalysis for the period from 1960 to 2015.

The station-based, daily meteorological records, here, precipitation and 2-m air temperature (maximum and minimum temperature) for the PLB are collected by the China Meteorological Administration (CMA) and are retrieved from the China Meteorological Service Network (https://data.cma.cn/). The data quality and data homogeneity from the network have been checked and controlled by CMA, and in total, 27 meteorological stations over the PLB (see Table 1) are selected in this study with their geographical locations shown in Fig. 1. The monthly

Table 1
Information about the 27 meteorological stations used in this study.

ID	Latitude (°N)	Longitude (°E)	Elevation (m)	Sub-basin	Annual average precipitation (mm)
57,993	25.5	114.5	99	Ganjiang	2457
58,606	28.4	115.58	27	Ganjiang	2632
58,634	28.4	118.15	93.6	Xinjiang	2869
57,799	27.05	114.55	72	Ganjiang	2543
57,598	29.02	114.34	121	Xiushui	2603
57,793	27.51	114.21	101	Ganjiang	2648
58,527	29.1	117.15	41.3	Raohe	2811
58,626	28.17	117.06	42	Xinjiang	2921
58,715	27.33	116.36	76.5	Fuhe	2757
58,813	26.45	116.06	320	Ganjiang	2791
58,506	29.35	115.59	1215	Poyang Lake	3031
58,519	29.01	116.4	25.8	Poyang Lake	2654
58,520	29.55	117.5	140.4	Raohe	2804
58,806	26.22	115.5	191	Ganjiang	2802
59,092	24.53	114.46	208	Ganjiang	2575
58,419	29.35	116.48	17.6	Poyang Lake	2626
58,507	29.16	115.05	58.6	Xiushui	2513
58,600	28.51	115.22	30	Ganjiang	2713
58,608	28.01	115.22	57.6	Ganjiang	2708
58,637	28.26	117.54	80	Xinjiang	2858
58,718	27.12	116.23	90.6	Fuhe	2801
58,500	29.5	115.1	36.9	Xiushui	2464
58,818	26.14	116.38	358.9	Ganjiang	2826
58,622	28.51	117.34	56.3	Xinjiang	2970
57,696	28.25	114.47	72.4	Ganjiang	2779
57,894	26.38	114.06	145	Ganjiang	2924
58,705	27.21	115.25	59	Ganjiang	2701

accumulated precipitation and the monthly mean of 2-m air temperature are then calculated from the daily records.

For the analysis of droughts associated ocean-atmospheric interactions, six climate indices are selected in this study according to the results of our literature research and preliminarily analysis of the corresponding relations with the basin-scale, monthly meteorological variables (Liu et al., 2020; Wu et al., 2020; Xiao et al., 2016): the El Niño/Southern Oscillation (ENSO), the Pacific Decadal Oscillation (PDO), the Atlantic Multidecadal Oscillation (AMO), the Arctic Oscillation (AO), the North Atlantic Oscillation (NAO), and the Indian Ocean Dipole (IOD). The selected six climate indices represent major climate variabilities in the Northern Hemisphere, which play crucial roles in modulating regional climate systems, particularly for the monsoon-controlled region (Das et al., 2020, 2022). Here, ENSO is referred to as anomalies of SST in the Niño 3.4 region (5°N–5°S, 120°W–170°W). The impact of ENSO on East Asian Monsoon is primarily through the modulation of the Walker circulation, which affects the strength and position of the monsoon trough. PDO is the SST anomalies in the Pacific north to 20°N (Mantua et al., 1997). Its influence on the East Asian monsoon is associated with the modification of the strength and position of the Pacific subtropical high, which in turn affects the moisture transport and precipitation over East Asia. AMO is the variability of SSTs of the North Atlantic Ocean (70°N–0° N) on the timescale of several decades (Enfield et al., 2001). AMO influences the East Asian monsoon through changing the Atlantic meridional overturning circulation. AO is defined using the monthly 1000 hPa geopotential height anomalies from the latitudes 20°N to 90°N, and the anomalies are then projected onto the AO loading pattern that is defined as the first empirical orthogonal function (EOF) of monthly mean 1000 hPa geopotential height (Thompson and Wallace, 1998). A positive AO phase is associated with a stronger polar vortex, which can lead to a northward shift of the jet stream, potentially affecting the monsoon onset and intensity. NAO is defined as the normalized pressure difference in the atmosphere at sea level between the Azores High and the Icelandic Low (Moore et al.,

2013). A positive NAO phase is associated with stronger westerlies over the Atlantic, which can influence the East Asian region by altering the strength of the Siberian High. IOD is defined as SSTs anomalies between the western equatorial Indian Ocean (50°E–70°E, 10°S–10°N) and the southeastern equatorial Indian Ocean (90°E–110°E, 10°S–0°N), and is also referred to as Dipole Mode Index (Saji et al., 1999). Its teleconnection to the East Asian monsoon is through the modification of the Indian monsoon and the associated cross-equatorial flow, which can influence the East Asian summer monsoon by altering the thermal gradient between the Indian Ocean and the Asian continent. ENSO, NAO, AO, and AMO are provided by the Climate Prediction Center (CPC) of United States National Oceanic and Atmospheric Administration (NOAA) (https://www.cpc.ncep.noaa.gov/data/). PDO and IOD are provided by the Earth System Research Laboratory of NOAA (https://psl.noaa.gov/gcos_wgsp/Timeseries/) and by the Japan Agency for Marine-Earth Science and Technology (JMASTEC) (https://www.jamstec.go.jp/e/about/informations/notification_2021_maintenance.html), respectively.

Furthermore, to understand the plausible atmospheric processes underlying the combined and lagged influences of the selected climate indices on regional droughts, the 850 hPa horizontal winds and the 500 hPa geopotential height from the National Centers for Environmental Prediction/National Centers for Atmospheric Research (NCEP-NCAR) reanalysis are used for composite analysis. The atmospheric reanalysis has a spatial resolution of 2.5° and a highest temporal resolution of 6-hourly. The monthly values for the 850 hPa winds and the 500 hPa geopotential height are obtained from the online climate/weather database of the NOAA Physical Sciences Laboratory (PSL) (https://psl.noaa.gov/data/gridded/data.ncep.reanalysis.html). The anomalies of the atmospheric variables are calculated by removing the climatological mean from 1960 to 2015.

2.3. Methodology

Fig. 2 shows the schematic flowchart of the methods applied in this study, and, accordingly, we follow a three-fold approach: Firstly, the Pearson's correlation coefficient is used to analyze the linear correlations between meteorological droughts and each climate oscillation; Secondly, the cross-wavelet transform is performed to address the non-
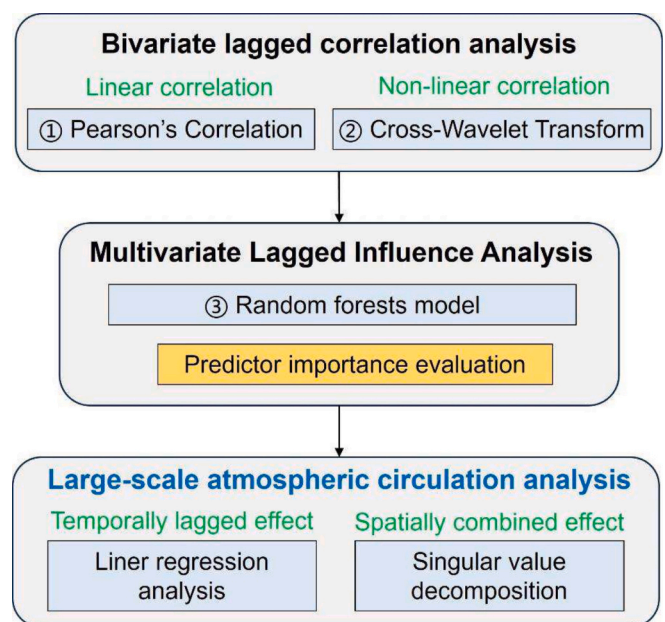
Fig. 2. A schematic workflow of this study including the performed analyses and the applied methods, accordingly.

linear correlations and the periodicity at multiple time scales; third, the random forests model is established and the variable sensitivity is analyzed to reveal the combined influences of multiple climate oscillations. All of the above-mentioned approaches are using the Standardized Precipitation Evapotranspiration Index (SPEI) as a drought metric. It is worth to note that the correlation analyses performed in this study particularly take the temporally lagged influences into account by setting changed time lags from 1 to 12 months. Lastly, the linear regression model and the singular value decomposition are employed to quantitively understand the relationship between the atmospheric circulations and the identified climatic indices, in order to elucidate the physical mechanisms behind the spatially combined and temporally lagged influences.

2.3.1. Meteorological droughts analysis

In this study, the term "drought" is related to meteorological drought, i.e. negative and short-term precipitation anomaly. The SPEI is a standardized and multi-timescale index that can fulfill the requirements for drought analysis in different regions under different climatic conditions (Chiang et al., 2021; Das et al., 2023; Vicente-Serrano et al., 2010, 2012; Yu et al., 2014). For the calculation of SPEI, we closely follow the studies of Vicente-Serrano et al. (2010) and Yu et al. (2014). The SPEI accounts for precipitation and potential evapotranspiration (PET) (Vicente-Serrano et al., 2010), and is derived by considering supply and demand of the water balance equation based on the probabilistic distribution function (Vicente-Serrano et al., 2010, 2020).

As a follow up to our previous study of Xing et al. (2022), we use the SPEI at the 3-month time scale to analyze the seasonal features of meteorological droughts over the PLB (Huang et al., 2019; Liu et al., 2020; Xu et al., 2015). The empirical Thornthwaite (TH) equation is used to calculate the PET for the reasons of its relatively simple concept (Thornthwaite, 1948) and its comparably wide applicability to our study region and its surrounding regions (Chen and Sun, 2015; Liu and Liu, 2019; Sun et al., 2020; Wu and Chen, 2019; Xu et al., 2015; Zhou et al., 2021).

2.3.2. Bivariate lagged correlation analysis

2.3.2.1. Pearson's correlation.
Pearson's correlation coefficient (PCC, (Da Silva et al., 2016) is used in this study to statistically quantify the linear relationship between monthly time series of lagged values of the selected climate indices φ_i and the SPEI ρ_i averaged over the PLB:

$$PCC = \frac{\sum\limits_{i=1}^{n} (\varphi_i - \overline{\varphi})(\rho_i - \overline{\rho})}{\sqrt{\sum\limits_{i=1}^{n} (\varphi_i - \overline{\varphi})^2} \sqrt{\sum\limits_{i=1}^{n} (\rho_i - \overline{\rho})^2}} \tag{1}$$

where n is the length of time series. The value of PCC ranges from -1 to 1 and positive values mean positive influences of the climate indices on the SPEI, and vice versa. The greater the absolute value of PCC, the stronger the linear correlation is. The Student's t-test using error probability of alpha $= 0.05$ is applied here to test the hypothesis of the "significance of the correlation coefficient".

2.3.2.2. Cross-wavelet transform.
Cross-wavelet transform (XWT, (Torrence and Compo, 1998) is employed in this study to investigate the nonlinear relationship between the selected climate indices and the SPEI in time-frequency domain at multiple time scales. XWT is chosen as it combines wavelet transformation with cross spectrum analysis so as to account for the nonstationary of two time series (Grinsted et al., 2004). The XWT of two time series $x(t)$ and $y(t)$ is defined as:

$$W_{xy} = W_x W_y^* \tag{2}$$

where W_x and W_y are the wavelet transform of x and y, respectively, and * denotes complex conjugation.

Accordingly, the wavelet coherence ρ_{xy} of two time series $x(t)$ and $y(t)$ is written as:

$$\rho_{xy} = \frac{S(W_{xy})}{\sqrt{S(|W_x|^2) S(|W_y|^2)}} \tag{3}$$

where S denotes a smoothing operator both in time and along the wavelet scale (Torrence and Compo, 1998). The phase difference ϕ_{xy} of two wavelets is calculated by

$$\phi_{xy} = arctan\left(\frac{\mathscr{I}[S(W_{xy})]}{\mathscr{R}[S(W_{xy})]}\right) \tag{4}$$

where $\mathscr{R}$ and $\mathscr{I}$ represent the real and imaginary parts of the spectra, respectively (Liu, 1994). The derived wavelet coherence of Eq. 3 and phase difference of Eq. 4 allow for estimations of the amplitude and time-varying periodicity in time-frequency domain between two non-stationary time series. In this study, the Morlet wavelet is chosen as the mother wavelet for XWT because of its effectiveness in extracting statistical features (Grinsted et al., 2004), such as analyses in the low-frequency domain, e.g., biennial, inter-annual, and decadal variations (Shao et al., 2017; Yang et al., 2012).

2.3.3. Multivariate lagged influence analysis

In order to further investigate the joint influence of multiple climate indices on meteorological droughts, a machine learning approach, the random forests (RF) model (Breiman, 2001) is employed in this study. The RF model is an ensemble learning method for classification and regression analyses. The concept of the RF model is to construct ensemble trees by randomly growing a collection of trees from bootstrap samples and aggregating predictions so as to improve robustness and reliability of regression trees. As the RF model has the advantages of fast training speed, high accuracy, and unsensitive to the size of training data, it has been intensively applied in numerous fields of geophysics, such as, landslides, floods, earthquakes, and soil erosions (Breiman, 2001; Chen et al., 2012; Konapala and Mishra, 2020; Li et al., 2020a; Zhu et al., 2020b).

In this study, we follow the study of (Feng et al., 2020) to consider the lagged influence of multiple climate indices, i.e., using predictors with varied time lags as inputs for the RF model. Specifically, the selected climate indices (ENSO, AMO, PDO, AO, NAO, and IOD) and initial SPEI (predictors) are the input variables of the RF model and the future SPEI is the output variable (predictand). To further investigate the role of different lead times (LT), that is referred to as "time distance" between the issuance of the forecast and the occurrence of meteorological droughts that are predicted (Arnone et al., 2020), in our lagged influence analysis, four RF models with the LT of 1-, 3-, 6-, and 9-month are trained. For each RF model with one selected LT, the relationship between predictors and predictand is simplified as follows:

$$SPEI_t = f(SPEI_{t-LT}, AO_{t-LT}, AO_{t-LT-1}, \cdots, AO_{t-12},$$

$$AMO_{t-LT}, AMO_{t-LT-1}, \cdots, AMO_{t-12},$$

$$ENSO_{t-LT}, ENSO_{t-LT-1}, \cdots, ENSO_{t-12},$$

$$IOD_{t-LT}, IOD_{t-LT-1}, \cdots, IOD_{t-12},$$

$$NAO_{t-LT}, NAO_{t-LT-1}, \cdots, NAO_{t-12},$$

$$PDO_{t-LT}, PDO_{t-LT-1}, \cdots, PDO_{t-12}) \tag{5}$$

where $SPEI_{t-LT}$ represents the initial condition of the forecasting model. $ENSO_{t-LT}, ENSO_{t-LT-1}, \cdots, ENSO_{t-12}$ represent the ENSO values with

time lags from LT to 12 months, respectively. The same applies to AO, AMO, IOD, NAO, and PDO.

It is worthy to note that taking all selected climate indices into one model of Eq. 5 allows for assessing multivariate lagged relationships. For the quantification, we use predictor importance to disentangle the impacts of different climate indices on meteorological droughts. The predictor importance reveals the importance of the randomly permuting predictors to the model accuracy by ranking the correspondingly decreased prediction accuracy (Bachmair et al., 2016; Wang et al., 2020a), is calculated as the change in percentage of the mean squared error (MSE):

$$MSE = \frac{1}{n} \sum_{i=1}^{i=n} (y_i - \widehat{y}_i)^2 \qquad (6)$$

where y_i and $\widehat{y}_i$ are the observed and modeled SPEI of each time step; n is the length of the time series. Higher MSE change means more important the climate index is to the meteorological droughts. The statistical significance of the predictor importance is tested using one-sided binomial test.

3. Results

3.1. Influence of individual climate indices on meteorological droughts

3.1.1. Bivariate lagged linear correlation

Fig. 3 displays the PCC between the selected climate indices (PDO, NAO, IOD, ENSO, AO, AMO) and the basin-averaged SPEI over the PLB for 1960–2015, with a time lag from 0 (no lag) to 12 months. In general, the linear correlations between the six climate indices and the meteorological droughts over the PLB are relatively low and non-significant with no consideration of time lag (i.e., lag = 0), whereas higher and significant correlations are found when the time lags are taken into account (i.e., lag >0). The values of PCC for each climate indices vary with time lag. The highest positive and significant correlations of SPEI are found with ENSO at a lag of 3–6 months, and the highest negative and significant correlations are with NAO at a lag of 2–3 months. Moreover, the signs of PCC for NAO, AO, AMO changes with time lags. For example, the direction of the relationship between NAO and the SPEI is negative and statistically significant at a lag of 1–3 months and becomes positive and statistically significant at a lag of 6–9 months. Similar as the pattern of the lagged correlations of NAO with the SPEI, AO is negatively correlated with the SPEI in adjacent half year (1–5 months) and positively correlated when the time lag is longer than 6 months (7–12 months), but the relationship is statistically significant mostly for a lag of 8 and 9 months. In the case of PDO and IOD, the sign

of the relationship between them and the SPEI are positive across all the considered time lags. Overall, the performed bivariate linear correlation analysis has identified that ENSO and NAO have the strongest lagged correlation with the SPEI (the best case explains 25% of the total variance), and PDO, AO, and AMO rank in the second tier. The linear correlation between IOD and the SPEI is negligibly low.

3.1.2. Bivariate lagged non-linear correlation

In this section, the lagged non-linear correlation between the selected climate indices and the SPEI is statically quantified by performing the XWT analysis of Section 2.3.2.2, and the results of the wavelet spectrum coherence (in color) and phase differences (arrows) are shown in Fig. 4.

More than six significant coherence peaks with different durations (around the periodicity bands of 8–16 months, 18–64 months, and 20–36 months) are found for the wavelet coherence of AMO-SPEI, and the corresponding phase differences within the identified coherence peaks of AMO-SPEI are dominantly in-phase except for the anti-phase around the periodicity of 8–16 months during 2000–2015 (Fig. 4a). In the case of the AO-SPEI (Fig. 4b), the significant coherence is found mostly around the 10–15 months bands during 1960–1965. ENSO has a significantly positive correlation with the SPEI around the periodicity of 16–48 months during 1970–1988 and 1990–2000, and their averaged phase differences implies that ENSO leads to the meteorological droughts over the PLB by around 9.4 months (Fig. 4c). Fig. 4d shows that the periodicity of the significant coherences between the case of IOD and the SPEI is around 24–40 months during 1968–1980 and 1992–1998. In the case of NAO, significantly negative correlation with the SPEI is found around the periodicity of 10–16 months during 1960–1970 and 24–40 months during 2005–2015 (Fig. 4e), while in the case of PDO significantly positive correlation is around the 48–64 months during 1985–2015 (Fig. 4f).

In addition, the effects of different climatic modes on local climate variability can be classified by comparing the significant coherence patterns of different climate indices. For example, ENSO and IOD have the similar significant coherence pattern (IOD has weaker coherence) which is around 16–48 months periodicity. The pattern of AO and NAO also similar to each other, which share the same significant zone of 8–16 months periodicity. Hence, ENSO and IOD, NAO and AO can be categorized as two pairs with similar local influence patterns. That corresponding to their spatially modes and physical meanings which is, ENSO and IOD represent tropical SSTA, while NAO and AO indicate mid- and high-latitude atmospheric circulation anomalies.

Table 2 summarizes the averaged values of the phase-angles (i.e., time lag) within the XWT-identified areas of significance around the
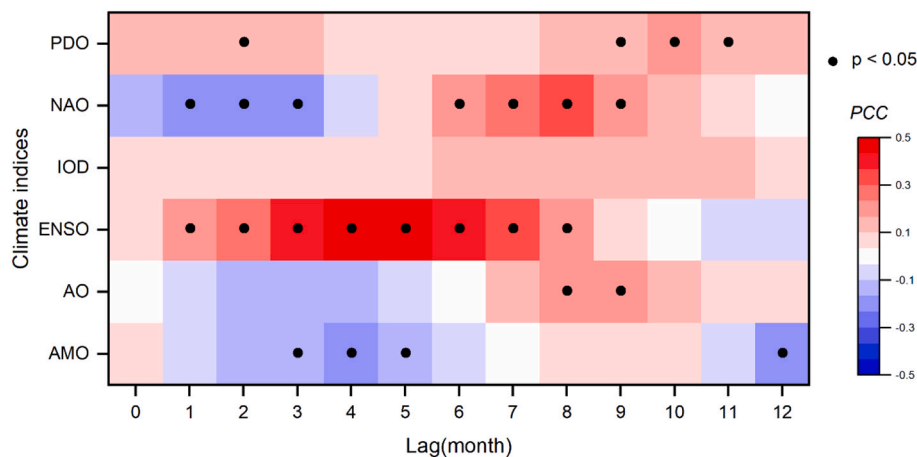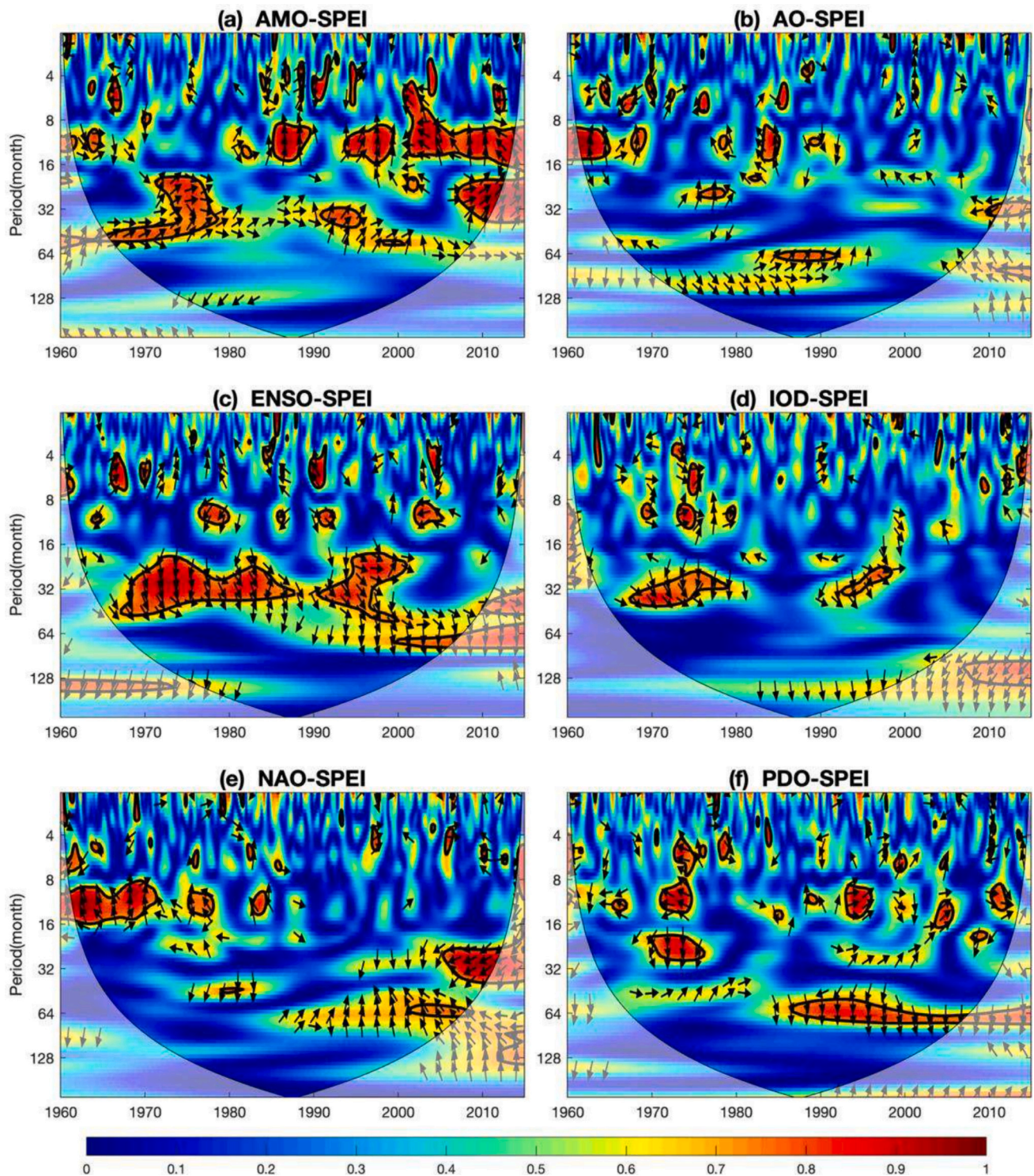

Fig. 3. Pearson's correlation coefficient between the selected climate indices (PDO, NAO, IOD, ENSO, AO, AMO) and the basin-averaged SPEI over the PLB for 1960–2015, with a changed time lag from 0 to 12 months. Superimposed dots indicate that the correlations are statistically significant at the 95% confidence level.

Fig. 4. Wavelet coherence (in color) and phase difference (arrows) between (a) AMO, (b) AO, (c) ENSO, (d) IOD, (e) NAO, (f) PDO and the SPEI averaged over the PLB for 1960–2015. The thick black contour indicates the 95% confidence level against the red noise, and the cone of influence is shown as the lighter shade. The color ranging from blue to red represents the spectrum coherence changing from weaker to stronger. Arrows pointing to the right direction denote in-phase, and the left direction stands for antiphase. Arrows upwards indicate the phase lag of the SPEI to the climate indices by $\pi/2$, and the arrows downwards indicate the phase lead of the SPEI to the climate indices by $\pi/2$. (For interpretation of the references to color in this figure legend, the reader is referred to the web version of this article.)

specific wavelengths, which represent the propagation time from different climatic modes to the local climate conditions over the PLB. Overall, the SPEI statistically responds to ENSO, IOD, and PDO with relatively longer time lags (> 9 months) and to NAO with a shorter time lag (around 4.6 months). Hence, we can infer that across temporal scales the SPEI of the PLB promptly responds to the variations of NAO,

followed by AMO and AO, but relatively slowly responds to those of ENSO, IOD, and PDO.

3.2. Influence of combined climate indices on meteorological droughts

In this section, the combined influence of the multiple climate

Table 2
Time lag (month) between the selected climate indices and the SPEI.

Climate index	Time lag (month)
AMO	6.1
AO	6.6
ENSO	9.4
IOD	10.6
NAO	4.6
PDO	11.7

Note: The time lags are calculated by the average phase angle within the XWT-identified areas of significance around the specific wavelengths in Fig. 4.

indices on the meteorological droughts for the PLB is evaluated by using the RF model of Section 2.3.3. Accordingly, the degree of importance of the involved climate indices at four different LTs (here, at 1, 3, 6, and 9 months) is shown in Fig. 5. It is found that, among the six climate indices, ENSO is the most important ranking index at all four LTs, followed by NAO, AO, and IOD. The test for statistical significance indicates that at shorter LTs (e.g., LT = 1 month) the meteorological droughts forecasting for the PLB is strongly influenced by NAO and AO, and at medium and longer LTs (LT ≥ 3 months) the forecasting is dominantly driven by ENSO with the modulations of NAO, AO, and IOD. In terms of the identified time lags, ENSO has the significant lagged influences on the SPEI when the time lags are 3, 6, and 11 months at the LTs longer than 3 months. By contrast, NAO and AO have a wider range of the lagged influence, i.e., from 2 months to 9 months, and the degree of importance of NAO and AO to the SPEI decreases with the LT becomes longer. In addition, IOD is identified to have significant influences on the SPEI at all four LTs but with relatively longer time lags (9–12 months).

### 3.3. Synthesis of combined and lagged influences results

Regarding the spatially combined influences, both the results of the RF model-quantified predictor importance (Fig. 5) and the Pearson's lagged correlations (Fig. 3) generally agree about that ENSO and NAO are the most pronounced forcing for the meteorological conditions over the PLB. Regarding the temporally lagged influences, the time lags quantified by the bivariate linear and nonlinear analysis of Section 3.1 and by the multivariate nonlinear analysis of Section 3.2 are mostly overlapped. Specifically, we find that ENSO is the primary teleconnection mode out of the selected six climate indices and has

significant influence on the meteorological droughts for the PLB. Among the various antecedent intervals, the ENSO with lags ranging from 3 to 6 months (positively correlated with SPEI) or 11 months (negatively correlated with SPEI) is one of major drivers likely triggering the following dry or wet transformation. In addition to ENSO, the NAO with lags of 2, 3 (negatively correlated with SPEI), and 8, 9 (positively correlated with SPEI) months also detected as an important modulator closely related to dryness/wetness of the PLB.

It is noticed that the RF model also highlights the importance of IOD and AO. However, the bivariate analysis (Fig. 3 and Fig. 4) shows IOD (AO) has similar correlation patterns (for both liner or non-liner correlation) with ENSO (NAO). The correlation magnitude of IOD (AO) with SPEI is lower than that of ENSO (NAO). Therefore, the teleconnection effects of IOD (AO) on climate condition of PLB are similar with ENSO (NAO) and can be represented by ENSO (NAO). Actually, NAO and AO are highly overlapped (correlation coefficient is 0.63 with $p < 0.05$) and both of them represent the main mode of low-frequency variability of the high-latitudes extratropical atmosphere (Báez et al., 2013; Rogers and McHugh, 2002). In that sense, NAO is considered more physically relevant and robust with the Northern Hemisphere variability than the AO (Ambaum et al., 2001). In addition, many studies demonstrate an observable or modeled cross-correlation characteristics between ENSO and IOD (Pillai et al., 2021; Stuecker et al., 2017; Wang et al., 2019; Yuan and Li, 2008), and the correlation coefficient of 0.31 ($p < 0.05$) also verifies the closely coupled relationship between them, which both arise from inherent dynamical instabilities in the coupled tropical low-latitudes air/sea system (Behera et al., 2006; Lestari and Koh, 2016). Overall, ENSO and NAO are extracted from the multiple climate oscillations as the dominant mode of interannual climate variability to represent the spatially combined teleconnections.

3.4. Associated atmospheric processes for the lagged influences of combined climate oscillations on regional droughts

It is found that changes in climate oscillations are generally characterized by being asymmetric in terms of phase and temporal evaluation (An et al., 2021). In this section, such asymmetric effects of climate oscillations on droughts over the PLB via teleconnection are further investigated by disentangling the atmospheric processes corresponding to the spatially combined and temporally lagged influences identified in Section 3.3. To this end, we regress the 850 hPa wind anomalies and the 500 hPa geopotential height anomalies onto each droughts-related climate oscillations (here, the detrended ENSO and the detrended
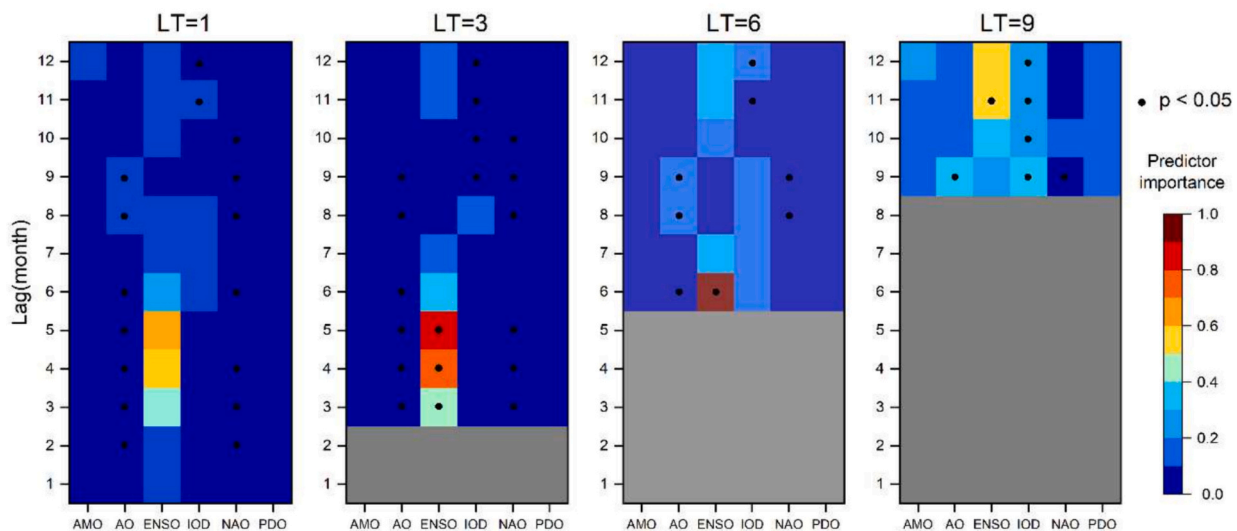
Fig. 5. The degree of importance of the selected climate indices to the SPEI, four lead times, which is estimated by the RF model at four LTs (i.e., 1-, 3-, 6-, and 9-month) for the lags from 1 month to 12 months. Superimposed dots indicate that the importance values are statistically significant at the 95% confidence level.

NAO) with the relevant time lags to disentangle the atmospheric circulation anomalies induced by individual climate oscillations (Fig. 6 and Fig. 7). Moreover, we apply the Singular Value Decomposition (SVD) analysis (Björnsson and Venegas, 1997) to the detrended and standardized 500 hPa geopotential height and the detrended and standardized SPEI over the PLB for October, when droughts over the PLB most frequently occur, to disentangle the drought-related atmospheric circulation patterns and their linkages with ENSO and NAO (Fig. 8).

3.4.1. Atmospheric circulation anomalies induced by ENSO and NAO

Fig. 6(Fig. 7) shows the regression patterns of 500 hPa geopotential height anomalies and 800 hPa wind anomalies against ENSO (NAO) with varied time lags, which generally reveals the lagged responses of drying- or wetting-prone atmospheric conditions over the PLB to ENSO (NAO).

In comparison to the regression pattern without the consideration of time lag (Fig. 6a), the anomalous cyclone over the western North Pacific (WNPC) at the time lag of 3 months (Fig. 6b) reinforces, extends westwards, and reaches areas close to the Lake Baikal region. Correspondingly, the west Pacific subtropical high (WPSH) is inhibited by the strengthened WNPC and the monsoonal southwesterlies over South China become stronger. Thus, abundant moisture from the South China Sea and the Bay of Bengal could be conveyed mostly through the junction zone between the higher- and lower-pressure circulation patterns, which are favorable for the wetting atmospheric condition over the PLB. At the lag of 6 months (Fig. 6c), the WNPC starts to be weakened and the northern ridge of the WPSH continues to extend northwards, which results in an anomalous high-pressure center over Northeast China.

Under such pattern, the PLB is still dominated by anomalous southwesterlies along the western edge of the WPSH.

At the lag of 11 months (Fig. 6d), the anomalous high-pressure center over Northeast China detaches from the WPSH and migrates to Mongolia-Siberian Region, which leads to the formation of Siberian blocking High (SH) and the triggering of a positive Eurasia (EU)-like teleconnection pattern, i.e., a high-pressure anomaly centered around Lake Baikal and a low-pressure anomaly around the Ural Mountains (Wallace and Gutzler, 1980). Such pattern leads to anomalous northerlies over East China including the PLB, in the south adjacent to the anomalous SH, and further weakens the East Asia summer monsoon (EASM). As a result, colder and drier air from the eastern side of the SH flows southwards along the Eastern China Plain passing by the PLB, and meanwhile warmer and wetter water vapor transported from the Indian Ocean and South Pacific towards the South China is reduced, which together leads to the occurrence of meteorological droughts over the PLB. Overall, the SH and EU-like atmospheric circulation patterns partly explain the atmospheric water deficits over the PLB, i.e., the high and negative relationship between the 11 months preceding ENSO and the SPEI over the basin (shown in Fig. 3).

Similar to Fig. 6, Fig. 7 shows the regression patterns against NAO with the time lag of 0, 2, 3, and 8 months. With the time lag changing from 0 to 2 months (comparing Fig. 7b to Fig. 7a), the NAO-induced mid-latitude high-pressure anomalies shrunk and move northwards. Meanwhile, the anomalous tropical cyclone over the South China Sea (SCSC) and the WNPC initiates and the wind anomalies over the PLB change from southeasterlies to northeasterlies. It is found that the regression pattern shown in Fig. 7b, i.e., anomalous high pressure
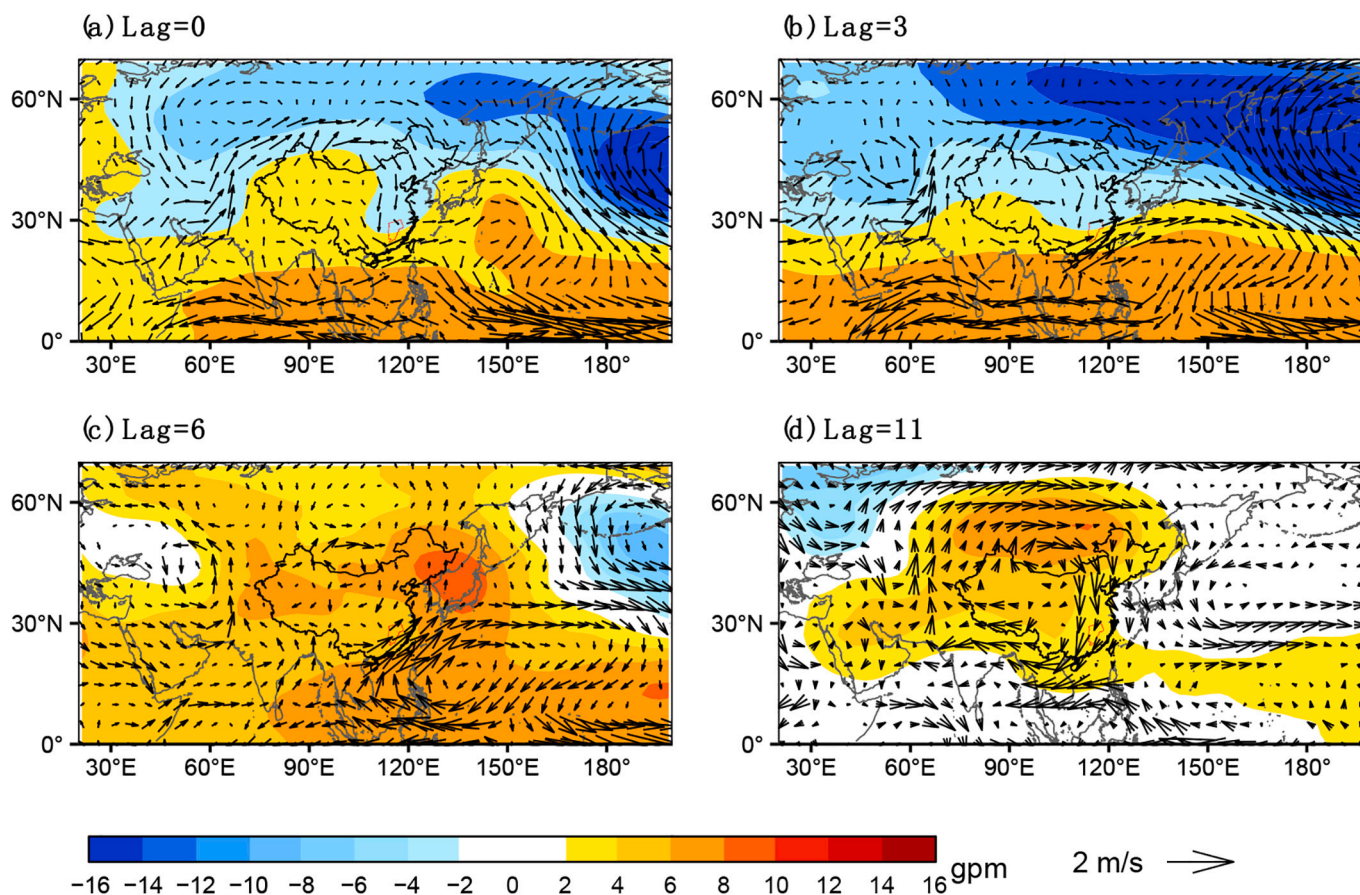

Fig. 6. Spatial patterns of the linear regression of the 500 hPa geopotential height anomalies (shading; gpm) onto the ENSO index for the period 1960–2015 with a time lag of (a) 0 month, (b) 3 months, (c) 6 months, and (d) 11 months. The arrows represent the linear regression of the 850 hPa wind anomalies onto the ENSO index (vector; m/s). The anomalies are derived based on the climatology for the period 1960–2015. The curved red line delineates the basin boundary of the PLB. (For interpretation of the references to color in this figure legend, the reader is referred to the web version of this article.)
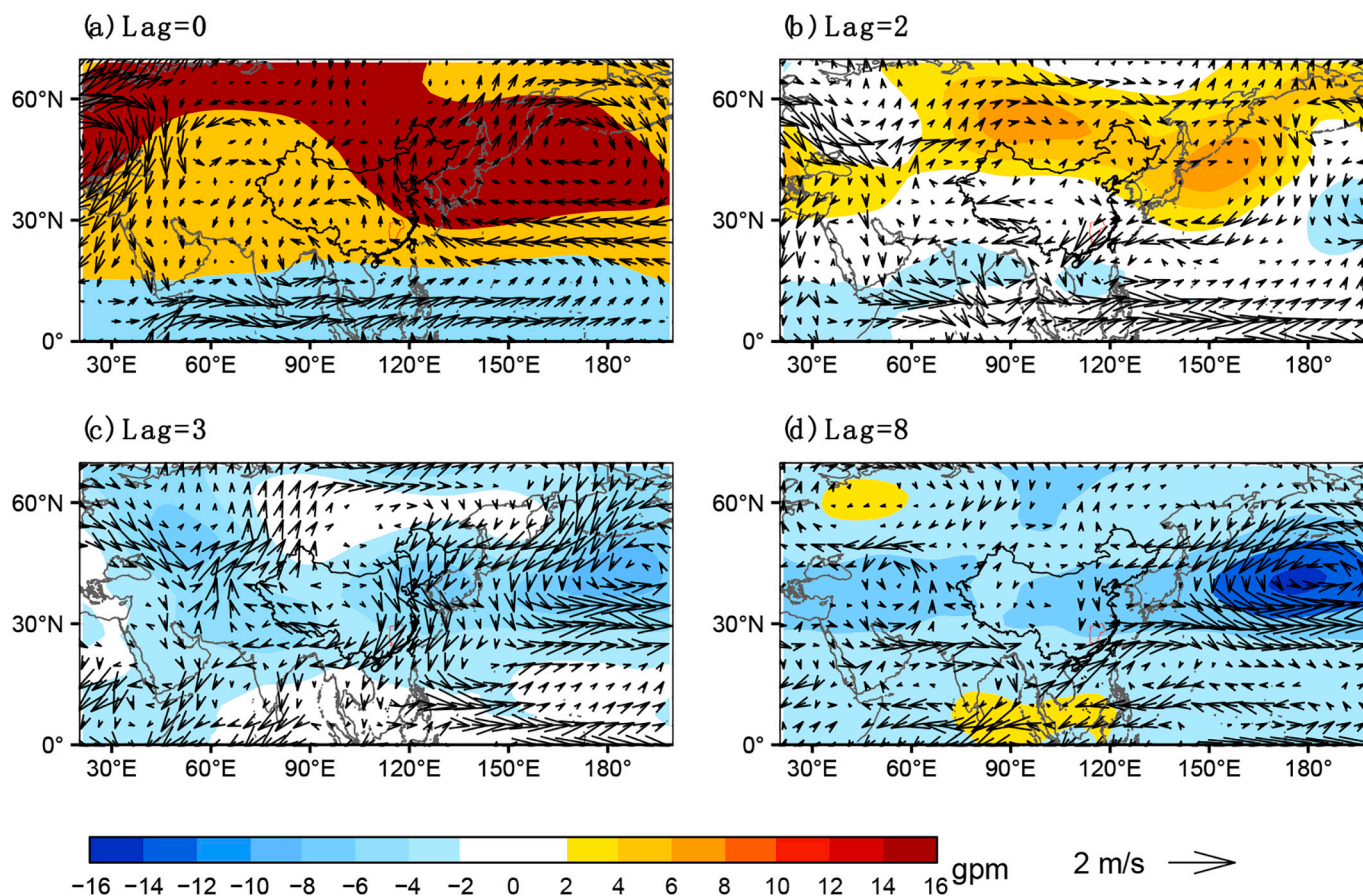
Fig. 7. As in Fig. 6, but onto the NAO index with the lags of (a) 0 month, (b) 2 months, (c) 3 months, (d) 8 months.

around Lake Baikal and low pressure centered in eastern East Asia, is similar to the positive EU pattern. At the lag of 3 months (Fig. 7c), the SH shown in Fig. 7b disappears, and the SCSC shifts northwards and merges together with the enhanced WNPC, so that the atmospheric moisture transport over entire East China is dominated by anomalous northerly currents. At the lag of 8 months (Fig. 7d), the coverage of the WNPC expands eastwards and low-latitude high pressure anomalies generate, causing the change of wind anomalies to southwesterly.

Overall, the performed regression analysis shows that ENSO with lag of 11 months and NAO with lag of 2–3 months trigger drought-prone circulation patterns over the PLB, which corresponds to the anti-phase correlation with the SPEI for the PLB; whereas ENSO with lag of 3–6 months and NAO with lag of 8 months arouse atmospheric circulation anomalies that facilitate precipitation generation over the PLB, which explains their in-phase correlation with the SPEI for the basin.

3.4.2. Autumn drought-related atmospheric circulation patterns induced by combined climate oscillations

To further examine the robustness of the PLB drought-associated atmospheric circulation patterns, e.g., positive EU-like patterns identified in Fig. 6d and Fig. 7b, and their combined linkages with ENSO and NAO, Fig. 8 depicts the results of the performed SVD analysis during 1981–2016 between the SPEI of 3-month timescale for October (i.e., frequently occurred early autumn droughts covering the period of August–September-October) for the PLB and the simultaneous 500 hPa geopotential height of Northern Hemisphere.
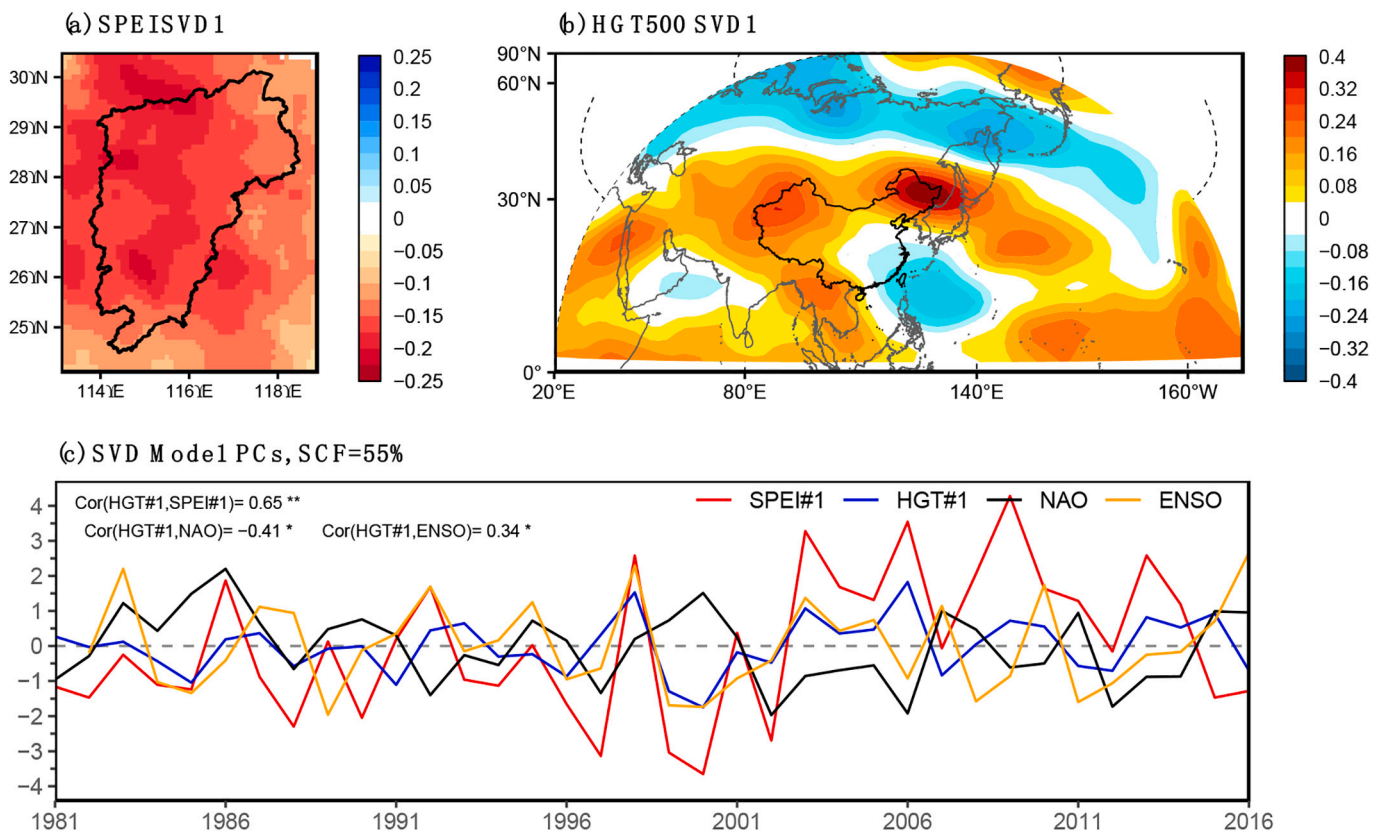
The heterogeneous correlations of SPEI for the first mode of SVD (SVD1) show a whole-basin drought pattern across the PLB (Fig. 8a). Correspondingly, a northwest-southeast "− + −" wave train originating from the Arctic Ocean and through Eurasia is apparently showed from the first mode geopotential height pattern (Fig. 8b), which closely

resembles the EU teleconnection pattern, with anomalous low pressure over the Kara Sea and East China Sea, and anomalous high pressure between them around Lake Baikal. Temporally, the evolutions for SPEI and geopotential height are significantly correlated with a coefficient of 0.65 ($p < 0.01$), suggesting that the first SVD mode of SPEI can well capture the autumn drought characteristic of PLB and is highly related to the EU pattern (explaining 55% of the total coupled variance). Moreover, the time series of SVD1 for geopotential height is significantly correlated with these of ENSO of December previous year and NAO of August current year, with correlation coefficients of 0.34 ($p < 0.05$) and − 0.41 ($p < 0.05$), respectively. That confirms the autumn drought-associated circulation anomalies are induced by preceding winter ENSO and late-summer NAO. Together with the in-phase (anti-phase) correlation between ENSO (NAO) and the SVD1 for geopotential height, it is inferred that the positive ENSO (El Niño) of preceding winter and negative NAO of late-summer jointly trigger autumn droughts over the PLB.

4. Discussions

4.1. Temporally lagged influence of climate oscillations

In this study, we disentangled the temporally lagged influence of multiple large-scale climate oscillations (i.e., AMO, AO, ENSO, NAO, PDO, and IOD) on the meteorological droughts over the PLB by conducting bivariate linear (Fig. 3) and non-linear (Fig. 4) correlation analysis as well as multivariate analysis (Fig. 5). In general, the results suggest that, among the six climate oscillation indices, the combined effects of preceding ENSO and NAO are the dominate drivers for the occurrence of meteorological droughts over the PLB. Our result is consistent with findings of previous studies about teleconnections over

Fig. 8. Atmospheric circulation patterns related to autumn droughts over the PLB. Heterogeneous correlation maps of the first SVD mode for the detrend and normalized (a) SPEI of October and (b) 500 hPa geopotential height (HGT), during 1981–2016, and (c) their corresponding normalized time series for the first SVD mode of SPEI and HGT, together with ENSO of preceding December and NAO of August. ** indicates the correlation is statistically significant at 99% confidence level, and * at 95% confidence level.

the PLB (Liu et al., 2020; Zhang et al., 2017). Moreover, our study quantitatively estimated that the lagged response time of the drying atmospheric conditions over the PLB to ENSO is about 11 months and to NAO about 2–3 months, while the response time of the wetting atmospheric conditions to ENSO is about 3–6 months, and to NAO about 8–9 months. Specifically, the autumn meteorological droughts over the PLB are triggered by the co-action of positive phase of preceding winter ENSO (El Niño) and negative phase of summer NAO.

In additional to the quantification of the relationship between the SPEI over the PLB and the six climate oscillation indices, we also disentangled the associated atmospheric circulation patterns with respect to two relevant indices (ENSO and NAO) and four different time lags (Fig. 6–8). The changes in the ENSO- and NAO-induced atmospheric circulation anomalies and horizontal wind anomalies with time lag further explain the plausible atmospheric mechanisms behind the derived temporally lagged relationship. We found that the co-occurrence of ENSO- or NAO- induced drought-prone circulation pattern, especially for autumn droughts over the PLB, is the enhancement of the anomalous anticyclone over the Lake Baikal and the attribution of the EU-like teleconnections. Such temporally lagged teleconnections have been found as well in numerous studies about extreme weather and climate events over regions in South China (Hu and Wang, 2021; Wang and Zhang, 2015; Xu et al., 2021). For instance, the occurrence of extreme rainfall events across the PLB is influenced mainly by ENSO occurring in the previous year and NAO in the same year (Zhang et al., 2014). Regarding seasonal droughts in the Yangtze River basin, (Huang et al., 2019) found that the SPEI there is significantly related to NAO and ENSO with lag of one year. On a continental scale, the rainfall pattern in the following summer over East Asia is significantly influenced by winter El Niño (Sun and Wang, 2019; Sun

et al., 2021; Wen et al., 2019).

Regarding the propagations from positive phase of preceding winter ENSO to extreme events in the PLB, numerous studies (Li et al., 2020b; Ma and Li, 2007; Yun et al., 2010) reveal that the mature phase of El Niño strongly modulates boreal winter Walker–Hadley circulations and meanwhile Indian Ocean SST warming is significantly maintained until summer, which consequently weakens WNPC and enhances the north-ward propagating Rossby waves, namely, the Pacific–Japan (PJ) pattern. When comparing with that of ENSO, we found that the propagation of NAO to extreme events in the PLB is more rapid. The lagged influences of negative phase of summer NAO on East Asia precipitation including the PLB have been reported in recent studies (Gu et al., 2009; Hong et al., 2022; Wang et al., 2018). It is found that the summer NAO primarily induces a triple North Atlantic SSTA persisting until autumn, and the SSTA thereby excites southeastward-propagating Rossby waves and induces a downstream plural zonal wave train (Han-Lie et al., 2013; Hu et al., 2022; Yuan et al., 2022), which explains the EU-like pattern shown in Fig. 8b.

4.2. Spatially combined effects of ENSO and NAO

The occurrence of regional meteorological droughts are often trig-gered by multiple drivers and modulators across the globe, such as anomalies of SST, sea ice, or snow cover, in association with persistently recurring atmospheric circulation anomalies that result in regional at-mospheric water deficits (Hao et al., 2018; Zhang et al., 2020b). Our previous study provides a robust evidence that drought events of the PLB are followed by strong ENSO episodes (Xing et al., 2022). In our present study, we found that, in additional to ENSO (Fig. 6), NAO (including AO) plays an important role in contributing to the drought-prone

atmospheric circulations over the PLB (Fig. 7). Recent studies also highlight that, NAO (AO) that describes high-latitude pressure variabilities induced by, e.g., changes in Eurasian snow cover and Arctic sea-ice cover, has more enhanced impacts on weather and climate extremes in the Northern Hemisphere, particularly under a warming climate (Tian and Fan, 2015; Wang et al., 2018; Zhou et al., 2022). For instance, (Chen et al., 2013) found the variation of winter temperature and precipitation in East Asia depends very much on the configuration of the AO and ENSO phases rather than only one of them: when negative phase of AO couples with positive phase of ENSO (a La Niña winter), a dipole pattern of the precipitation anomalies over East Asia with more rainfall in the coastal region of Southeast China and less rainfall in the Yangtze River valley including our study region is found. (Wang et al., 2017) found that extreme droughts in North China do not necessarily result from strong El Niño, but depend on the occurrence of a positive EU pattern induced by the synergistically involving of El Niño with reduced Eurasian spring snow cover. Regarding the recent long-lasting severe drought in South China during autumn -winter 2020/2021, (Sun et al., 2022) attributes it to the combined effects of La Niña and negative Arctic Sea ice anomalies and the induced anomalous Eurasian atmospheric wave-train.

Regarding the atmospheric teleconnection mechanisms, the EU-like "− + −" wave train is used in this study to describe the dominant joint effects of ENSO and NAO on regional extremes in the PLB (Fig. 6 and Fig. 7). For the drought-prone atmospheric circulation patterns, we found that in addition to the EU-like pattern a meridional PJ-like pattern over East Asia and the northwestern Pacific might play a secondary role in the propagation from ENSO via the Walker–Hadley circulation to the SPEI, with cyclones over the tropical western Pacific and anticyclones over the East China Sea and Japan (Nitta, 1987). We conclude that the plausible atmospheric causes for joint the spatially combined and temporally lagged effects of ENSO and NAO on seasonal droughts over the PLB is likely due to PJ-EU combined teleconnections bridging Pacific and Atlantic SSTA with the SPEI for the basin (Fig. 9), which is supported by recent studies (Hu et al., 2020; Wang and He, 2015).

4.3. Implications for the seasonal drought forecasting

Regional droughts occurring at seasonal and sub-seasonal scales have been becoming one of the most globally recognized threats to the sustainable development of such as environment, society, and human heath (Rodriguez, 2022). It is reported that rivers and lakes are drying across the globe (Toreti et al., 2022). This is particularly the case in our study region PLB, where the largest freshwater lake of the country is. The extreme drought over the PLB in 2022 lasts >80 days, which results in a decreased lake area less to one ninth of its normal size and around 1 billion US dollar economic losses. However, skillful seasonal drought forecasting at regional scales is still a challenging question due to the complexity of drought occurrence with multiple drivers/modulators and the decreased predictability of methods for drought forecasting with leading time (Hao et al., 2018). Therefore, new awareness and consciousness of skillful regional drought forecasting across spatial and temporal scales are urgently needed. Recent community efforts in this direction have been made jointly by scientists, stakeholders, and decision-maker, for example, the Sub-seasonal to Seasonal prediction project, in order to bridge the gap between the short-term weather and long-term climate prediction (Pegion et al., 2019; Robertson et al., 2020; Vitart et al., 2012, 2017). It has been revealed that the enhanced understandings of the interactions among oceans, land, and cryosphere can potentially lead to an enhanced predictability, i.e., more skillful prediction of dynamical processes and their variabilities at seasonal and subseasonal scales (Cohen and Saito, 2003; Forootan et al., 2019; Hong et al., 2022). In this regard, our study highlights the different propagation times from multiple large-scale climate oscillations to regional climatic extremes, which could guide the identification of suitable predictors for skillful seasonal drought forecasting in other regions worldwide.

In this study, we have applied a consolidated univariate-to-multivariate analysis framework to systematically disentangle multiple large-scale climate oscillations on seasonal droughts over the PLB in terms of strength, direction, periodicity, and significance of the relationship. Pearson's correlation quantitively assesses linear relationships by calculating the strength and direction of correlations (Fig. 3), which sheds light on the positive or negative associations between climate indices and drought conditions. XWT allows us to identify periodic patterns in the influence of climate indices on droughts and to evaluate how these patterns evolve over time (Fig. 4), which is particularly applicable for understanding the non-stationarity in correlations. The RF model addresses the complex interactions among multiple variables (Fig. 5). The advantage of RF modeling is to evaluate variable importance, and to pinpoint the most influential climate indices among multiple variables. Although each method has its uniqueness in analyzing the climate oscillation-drought relationship, their results complement each other. Pearson's correlation offers a straightforward way to understand linear relationships, XWT uncovers nonlinear interactions across timescales, and the RF model tackles the complexity of
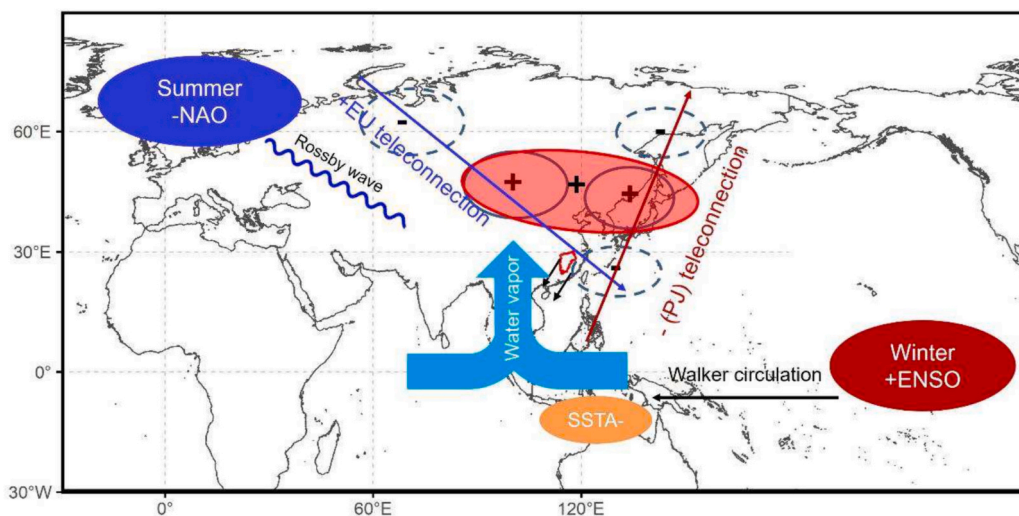

Fig. 9. Schematic diagram of the identified spatially combined and temporally lagged influences of the large-scale climate patterns induced by ENSO and NAO on the seasonal droughts in the Poyang Lake basin for the period of 1960–2015.

multivariate relationships. The statistically significant consensus among these methods enhances the credibility of our findings. For example, the Pearson's correlation and XWT analyses identify the important time lags at which the climate indices show significant correlation with the SPEI over the PLB (Section 3.1), and the RF modeling shows that ENSO, NAO, and AO with the specific lags dominate the variation of the SPEI at different lead times (Section 3.2). Moreover, the composite analysis reveals the bridging effect of the PJ-EU combined circulation patterns for the occurrence of regional droughts (Section 3.4).

In terms of autumn droughts over the PLB, we have found that the impacts of NAO are pronounced at a short lead (2–3 months), while ENSO is a precursor for long lead times (11 months). The transformation from wet-prone to dry-prone atmospheric circulation patterns following ENSO (Fig. 6) indicates that the early warning signal from ENSO for seasonal drought forecasting over the PLB can be extended up to almost one year. Besides, the co-action of ENSO and NAO imply that combing climatic oscillation signals at the high-latitude with these at the low-latitude can improve the seasonal forecast skill of regional extremes. It is expected that the derived predictive information about seasonal droughts over the PLB here can be adapted to dynamical and/or statistical forecasting models to achieve more skillful seasonal drought forecasting. Given the identified lagged influences of climate oscillations, such as ENSO and NAO, on droughts in the PLB, there is a need to enhance early warning systems by additionally monitoring changes in the identified climate indices. Early warning systems should be improved by explicitly considering the identified time lags in order to increase the lead time for drought management and adaptation (Dikshit et al., 2021). In this regard, potential policy recommendations for mitigating droughts include, such as, implementing climate forecasts information into regulation rules of reservoir operations (Giuliani et al., 2019), promoting water-saving agricultural practices (Xing et al., 2020), enhancing real-time monitoring systems (Zhang et al., 2019a, 2019b).

4.4. Limitation and future scope

The current study is subject to limitations. For example, although our consolidated univariate-to-multivariate analysis framework analysis provides insights into the dynamics of seasonal droughts occurrence and development, our findings analyzed only the most dominant two climate oscillations (ENSO and NAO) and our analysis period is restricted to 1960–2015. It is acknowledged that the disentangled empirical relationship has uncertainties due to the non-stationary of the climate systems. Such empirical relationship may change over time, particularly under the future warming conditions. Therefore, timely accommodating new datasets and evolving climate extremes, especially, in the real-time forecasting system would narrow this uncertainty. This study lays the groundwork for future research aiming at refining our understanding and model predictivity for climate extremes. One future research direction could be to integrate the derived statistical relationship between large-scale ENSO, NAO and regional droughts from the perspective of spatial correlations and time lags, in order to enhance the predictivity of seasonal drought forecasting systems. The overarching goal would be to develop a robust predictive framework that can provide reliable, timely, and actionable information to stakeholders, thereby aiding in the effective management and mitigation of drought risks.

5. Summary and conclusion

In this study, we have investigated the combined and lagged influences of large-scale climate patterns (AMO, AO, ENSO, IOD, NAO, and PDO) on climate extremes in the Poyang Lake basin (PLB) for the period of 1960–2015. The Standardized Precipitation Evapotranspiration Index based on monthly precipitation and temperature records from 27 meteorological stations is used to determine meteorological droughts over the basin. To statistically quantify such lagged and combined effects of teleconnections, Pearson's correlation coefficients, cross-

wavelet transform, and random forests model have been applied to perform a univariate-to-multivariate relation analysis. Moreover, associated atmospheric mechanisms for the spatially combined and temporally lagged influences of climate oscillations have been investigated by using the zonal and meridional wind fields at 850 hPa and the geopotential height at 500 hPa from the NCEP/NCAR reanalysis.

Our main results are summarized as follows:

1. The results of the univariate-to-multivariate analysis shows that, regarding spatially combined influences, the co-action of ENSO and NAO are the most important forcing for the meteorological conditions over the PLB. Regarding the temporally lagged influences, ENSO with lag of 11 months and NAO with lag of 2–3 months trigger droughts over the PLB; whereas ENSO with lag of 3–6 months and NAO with lag of 8–9 months arouse pluvial.
2. The results of lagged regression analysis correspond well with the statistical lagged relationship. ENSO with lag of 11 months and NAO with lag of 2–3 months trigger an EU-like drought-prone circulation patterns over the PLB, which is favorable for anomalous northerly currents and weakening the EASM. The wetness caused by 3–6 months lagged ENSO and 8 months lagged NAO is associated with the anomalous southerly currents induced by enhanced and eastwardly WNPC.
3. Our performed SVD analysis on the SPEI for the PLB and geopotential height reveals that the combined effect of preceding winter El Niño and late-summer negative NAO is the primary cause of autumn droughts over the PLB, which accompanied with a positive EU-like pattern.

Overall, it can be concluded that our findings improve the understanding of the physical mechanisms and drivers of seasonal droughts, which may be used as predictor variables in statistical drought forecasting models. However, it is noted that these statistical models are practically restricted by the underlying assumption of non-stationarity. Thus, frequent updates and recalculations of the statistical model equations are needed. In the future, a more detailed process-based modeling study using regional climate models will be conducted to gain further understanding of the impact of climate oscillations on regional extremes.

CRediT authorship contribution statement

Zikang Xing: Writing – original draft, Visualization, Software, Methodology, Investigation, Formal analysis, Data curation, Conceptualization. **Jianhui Wei:** Writing – review & editing, Supervision, Project administration, Funding acquisition, Conceptualization. **Yunliang Li:** Supervision, Resources, Project administration. **Xuejun Zhang:** Supervision, Funding acquisition. **Miaomiao Ma:** Funding acquisition. **Peng Yi:** Supervision. **Qin Ju:** Supervision. **Patrick Laux:** Writing – review & editing, Supervision. **Harald Kunstmann:** Writing – review & editing, Supervision, Resources, Project administration, Funding acquisition.

Declaration of competing interest

Data availability

The in-situ station data of precipitation and near-surface temperature can be publicly obtained from Meteorological Data Center of China Meteorological Administration (https://data.cma.cn/). Among the climate indices, ENSO, NAO, AO, and AMO are provided by the Climate Prediction Center of United States National Oceanic and Atmospheric Administration (https://www.cpc.ncep.noaa.gov/data/). PDO is

References

Abiy, A.Z., Melesse, A.M., Abtew, W., 2019. Teleconnection of regional drought to ENSO, PDO, and AMO: Southern Florida and the Everglades. Atmosphere (Basel) 10, 1–15. https://doi.org/10.3390/atmos10060295.

Ambaum, M.H.P., Hoskins, B.J., Stephenson, D.B., 2001. Arctic Oscillation or North Atlantic Oscillation? J. Clim. 14, 3495–3507. https://doi.org/10.1175/1520-0442(2001)014<3495:AOONAO>2.0.CO;2.

An, S.-I., Tziperman, E., Okumura, Y.M., Li, T., 2021. ENSO irregularity and asymmetry. In: McPhaden, M.J., Santoso, A., Cai, W. (Eds.), El Niño Southern Oscillation in a Changing Climate. American Geophysical Union, pp. 153–172.

Arnone, E., Cucchi, M., Gesso, S.D., Petitta, M., Calmanti, S., 2020. Droughts prediction: a methodology based on climate seasonal forecasts. Water Resour. Manag. 34, 4313–4328. https://doi.org/10.1007/s11269-020-02623-3.

Bachmair, S., Svensson, C., Hannaford, J., Barker, L.J., Stahl, K., 2016. A quantitative analysis to objectively appraise drought indicators and model drought impacts. Hydrol. Earth Syst. Sci. 20, 2589–2609. https://doi.org/10.5194/hess-20-2589-2016.

Báez, J.C., Gimeno, L., Gómez-Gesteira, M., Ferri-Yáñez, F., Real, R., 2013. Combined effects of the North Atlantic Oscillation and the Arctic Oscillation on sea surface temperature in the Alborán Sea. PLoS One 8, e62201. https://doi.org/10.1371/journal.pone.0062201.

Behera, S.K., Luo, J.J., Masson, S., Rao, S.A., Sakuma, H., Yamagata, T., 2006. A CGCM study on the interaction between IOD and ENSO. J. Clim. 19, 1688–1705. https://doi.org/10.1175/JCLI3797.1.

Berg, A., Sheffield, J., 2018. Climate change and drought: the soil moisture perspective. Curr. Clim. Chang. Rep. 4, 180–191. https://doi.org/10.1007/s40641-018-0095-0.

Björnsson, H., Venegas, S.A., 1997. A Manual for EOF and SVD Analyses of Climate Data. McGill University, Montréal, Québec.

Breiman, L., 2001. Random forests. Mach. Learn. 45, 5–32. https://doi.org/10.1007/978-3-030-62008-0_35.

Chen, H., Sun, J., 2015. Changes in drought characteristics over China using the standardized precipitation evapotranspiration index. J. Clim. 28, 5430–5447. https://doi.org/10.1175/JCLI-D-14-00707.1.

Chen, J., Li, M., Wang, W., 2012. Statistical uncertainty estimation using random forests and its application to drought forecast. Math. Probl. Eng. 2012, 1–13. https://doi.org/10.1155/2012/915053.

Chen, W., Lan, X.Q., Wang, L., Ma, Y., 2013. The combined effects of the ENSO and the Arctic Oscillation on the winter climate anomalies in East Asia. Chin. Sci. Bull. 58, 1355–1362. https://doi.org/10.1007/s11434-012-5654-5.

Chen, X., Li, F.W., Wang, Y.X., Feng, P., Yang, R.Z., 2019. Evolution properties between meteorological, agricultural and hydrological droughts and their related driving factors in the Luanhe River basin, China. Hydrol. Res. 50, 1096–1119. https://doi.org/10.2166/nh.2019.141.

Chiang, F., Mazdiyasni, O., AghaKouchak, A., 2021. Evidence of anthropogenic impacts on global drought frequency, duration, and intensity. Nat. Commun. 12, 1–10. https://doi.org/10.1038/s41467-021-22314-w.

Cohen, J.L., Saito, K., 2003. Eurasian snow cover, more skillful in predicting U.S. winter climate than the NAO/AO? Geophys. Res. Lett. 30, 10–13. https://doi.org/10.1029/2003GL018053.

Da Silva, R., Lamb, L.C., Barbosa, M.C., 2016. Universality, correlations, and rankings in the Brazilian universities national admission examinations. Physica A 457, 295–306. https://doi.org/10.1016/j.physa.2016.03.014.

Dai, A., 2011. Drought under global warming: a review. Wiley Interdiscip. Rev. Clim. Chang. 2, 45–65. https://doi.org/10.1002/wcc.81.

Das, J., Jha, S., Goyal, M.K., 2020. On the relationship of climatic and monsoon teleconnections with monthly precipitation over meteorologically homogenous regions in India: Wavelet & global coherence approaches. Atmos. Res. 238, 104889 https://doi.org/10.1016/j.atmosres.2020.104889.

Das, S., Das, J., Umamahesh, N.V., 2022. Investigating the propagation of droughts under the influence of large-scale climate indices in India. J. Hydrol. (Amst.) 610, 127900. https://doi.org/10.1016/j.jhydrol.2022.127900.

Das, S., Das, J., Umamahesh, N.V., 2023. A non-stationary based approach to understand the propagation of meteorological to agricultural droughts. Water Resour. Manag. 37, 2483–2504. https://doi.org/10.1007/s11269-022-03297-9.

Di Baldassarre, G., Martinez, F., Kalantari, Z., Viglione, A., 2016. Drought and flood in the anthropocene: modelling feedback mechanisms. Earth Syst. Dyn. Discuss. 1–24 https://doi.org/10.5194/esd-2016-65.

Dikshit, A., Pradhan, B., Alamri, A.M., 2021. Long lead time drought forecasting using lagged climate variables and a stacked long short-term memory model. Sci. Total Environ. 755, 142638 https://doi.org/10.1016/j.scitotenv.2020.142638.

Enfield, D.B., Mestas-Nuñez, A.M., Trimble, P.J., 2001. The Atlantic Multidecadal Oscillation and its relation to rainfall and river flows in the continental U.S. Geophys. Res. Lett. 28, 2077–2080.

Feng, P., Wang, B., Luo, J.J., Liu, D.L., Waters, C., Ji, F., Ruan, H., Xiao, D., Shi, L., Yu, Q., 2020. Using large-scale climate drivers to forecast meteorological drought condition in growing season across the Australian wheatbelt. Sci. Total Environ. 724, 138162 https://doi.org/10.1016/j.scitotenv.2020.138162.

Forootan, E., Khaki, M., Schumacher, M., Wulfmeyer, V., Mehrnegar, N., van Dijk, A.I.J. M., Brocca, L., Farzaneh, S., Akinluyi, F., Ramillien, G., Shum, C.K., Awange, J., Mostafaie, A., 2019. Understanding the global hydrological droughts of 2003–2016 and their relationships with teleconnections. Sci. Total Environ. 650, 2587–2604. https://doi.org/10.1016/j.scitotenv.2018.09.231.

Fung, K.F., Huang, Y.F., Koo, C.H., Soh, Y.W., 2020. Drought forecasting: a review of modelling approaches 2007–2017. J. Water Clim. Change 11, 771–799. https://doi.org/10.2166/wcc.2019.236.

Gao, T., Wang, H.J., Zhou, T., 2017. Changes of extreme precipitation and nonlinear influence of climate variables over monsoon region in China. Atmos. Res. 197, 379–389. https://doi.org/10.1016/j.atmosres.2017.07.017.

Giuliani, M., Zaniolo, M., Castelletti, A., Davoli, G., Block, P., 2019. Detecting the state of the climate system via artificial intelligence to improve seasonal forecasts and inform reservoir operations. Water Resour. Res. 55, 9133–9147. https://doi.org/10.1029/2019WR025035.

Gore, M., Abiodun, B.J., Kucharski, F., 2020. Understanding the influence of ENSO patterns on drought over southern Africa using SPEEDY. Clim. Dyn. 54, 307–327. https://doi.org/10.1007/s00382-019-05002-w.

Grinsted, A., Moore, J.C., Jevrejeva, S., 2004. Application of the cross wavelet transform and wavelet coherence to geophysical time series. Nonlinear Process. Geophys. 11, 561–566. https://doi.org/10.5194/npg-11-561-2004.

Gu, W., Li, C., Li, W., Zhou, W., Chan, J.C.L., 2009. Interdecadal unstationary relationship between NAO and East China's summer precipitation patterns. Geophys. Res. Lett. 36, 2–5. https://doi.org/10.1029/2009GL038843.

Guo, R., Zhu, Y., Liu, Y., 2020. A comparison study of precipitation in the Poyang and the Dongting Lake Basins from 1960-2015. Sci. Rep. 10, 1–12. https://doi.org/10.1038/s41598-020-60243-8.

Haile, G.G., Tang, Q., Li, W., Liu, X., Zhang, X., 2020. Drought: Progress in broadening its understanding. WIREs Water 7, 1–25. https://doi.org/10.1002/wat2.1407.

Han-Lie, X., Juan, F., Cheng, S., 2013. Impact of preceding summer North Atlantic oscillation on early autumn precipitation over Central China. Atmos. Ocean. Sci. Lett. 6, 417–422. https://doi.org/10.3878/j.issn.1674-2834.13.0027.

Hao, Z., Singh, V.P., Xia, Y., 2018. Seasonal drought prediction: advances, challenges, and future prospects. Rev. Geophys. 56, 108–141. https://doi.org/10.1002/2016RG000549.

Hermanson, L., Ren, H.-L., Vellinga, M., Dunstone, N.D., Hyder, P., Ineson, S., Scaife, A. A., Smith, D.M., Thompson, V., Tian, B., Williams, K.D., 2017. Different types of drifts in two seasonal forecast systems and their dependence on ENSO. Clim. Dyn. https://doi.org/10.1007/s00382-017-3962-9.

Hong, X., Guo, S., Xiong, L., Liu, Z., 2014. Spatial and temporal analysis of drought using entropy-based standardized precipitation index: a case study in Poyang Lake basin, China. Theor. Appl. Climatol. 122, 543–556. https://doi.org/10.1007/s00704-014-1312-y.

Hong, H., Sun, J., Wang, H., 2022. Interannual variations in summer extreme precipitation frequency over Northern Asia and related atmospheric circulation patterns. J. Hydrometeorol. 23, 619–636. https://doi.org/10.1175/JHM-D-21-0177.1.

Hu, Y., Wang, S., 2021. Associations between winter atmospheric teleconnections in drought and haze pollution over Southwest China. Sci. Total Environ. 766, 142599 https://doi.org/10.1016/j.scitotenv.2020.142599.

Hu, P., Cheng, J., Feng, G., Dogar, M.M.A., Gong, Z., 2020. The mechanism of EAP-EU combined impact on summer rainfall over North Asia. Theor. Appl. Climatol. 142, 117–128. https://doi.org/10.1007/s00704-020-03295-0.

Hu, Y., Zhou, B., Han, T., Li, H., Wang, H., 2022. In-phase variations of spring and summer droughts over Northeast China and their relationship with the North Atlantic Oscillation. J. Clim. 1–33 https://doi.org/10.1175/jcli-d-22-0052.1.

Huang, T., Xu, L., Fan, H., 2019. Drought characteristics and its response to the global climate variability in the Yangtze River Basin, China. Water (Basel) 11, 1–19. https://doi.org/10.3390/w11010013.

Jiang, P., Yu, Z., Acharya, K., 2019. Drought in the western United States: its connections with large-scale oceanic oscillations. Atmosphere (Basel) 10, 1–12. https://doi.org/10.3390/ATMOS10020082.

Kim, J.S., Seo, G.S., Jang, H.W., Lee, J.H., 2017. Correlation analysis between Korean spring drought and large-scale teleconnection patterns for drought forecasting. KSCE J. Civ. Eng. 21, 458–466. https://doi.org/10.1007/s12205-016-0580-8.

Konapala, G., Mishra, A., 2020. Quantifying climate and catchment control on hydrological drought in the continental United States. Water Resour. Res. 56, 1–25. https://doi.org/10.1029/2018WR024620.

Lestari, R.K., Koh, T.Y., 2016. Statistical evidence for asymmetry in ENSO–IOD interactions. Atmosphere-Ocean 54, 498–504. https://doi.org/10.1080/07055900.2016.1211084.

Li, Xiao, Li, D., Li, Xing, Chen, L., 2018. Prolonged seasonal drought events over northern China and their possible causes. Int. J. Climatol. 38, 4802–4817. https://doi.org/10.1002/joc.5697.

Li, Z., Chen, T., Wu, Q., Xia, G., Chi, D., 2020a. Application of penalized linear regression and ensemble methods for drought forecasting in Northeast China. Meteorog. Atmos. Phys. 132, 113–130. https://doi.org/10.1007/s00703-019-00675-8.

Li, Y., Liu, F., Hsu, P.C., 2020b. Modulation of the Intraseasonal Variability of Pacific-Japan Pattern by ENSO. J. Meteorol. Res. 34, 546–558. https://doi.org/10.1007/s13351-020-9182-y.

Lin, Q., Wu, Z., Singh, V.P., Sadeghi, S.H.R., He, H., Lu, G., 2017. Correlation between hydrological drought, climatic factors, reservoir operation, and vegetation cover in the Xijiang Basin, South China. J. Hydrol. (Amst.) 549, 512–524. https://doi.org/10.1016/j.jhydrol.2017.04.020.

Liu, P.C., 1994. Wavelet Spectrum Analysis and Ocean Wind Waves. NOAA Great Lakes Environmental Research Laboratory. ACADEMIC PRESS, INC. https://doi.org/10.1016/B978-0-08-052087-2.50012-8

Liu, W., Liu, L., 2019. Analysis of dry/wet variations in the Poyang Lake basin using standardized precipitation evapotranspiration index based on two potential evapotranspiration algorithms. Water (Basel) 11, 1–22. https://doi.org/10.3390/w11071380.

Liu, Y., Song, P., Peng, J., Fu, Q., Dou, C., 2011. Recent increased frequency of drought events in Poyang Lake basin, China: climate change or anthropogenic effects?. In: Proceedings of Symposium J-H02 Held during IUGG2011 in Melbourne, Australia, pp. 99–104.

Liu, Zhenchen, Lu, G., He, H., Wu, Z., He, J., 2018a. A conceptual prediction model for seasonal drought processes using atmospheric and oceanic standardized anomalies: Application to regional drought processes in China. Hydrol. Earth Syst. Sci. 22, 529–546. https://doi.org/10.5194/hess-22-529-2018.

Liu, Zhiyong, Zhang, X., Fang, R., 2018b. Multi-scale linkages of winter drought variability to ENSO and the Arctic Oscillation: a case study in Shaanxi, North China. Atmos. Res. 200, 117–125. https://doi.org/10.1016/j.atmosres.2017.10.012.

Liu, W., Zhu, S., Huang, Y., Wan, Y., Wu, B., Liu, L., 2020. Spatiotemporal variations of drought and their teleconnections with large-scale climate indices over the Poyang Lake Basin, China. Sustainability 12, 1–18. https://doi.org/10.3390/SU12093526.

Ma, J., Li, J., 2007. Strengthening of the boreal winter Hadley circulation and its connection with ENSO. Prog. Nat. Sci. 17, 1327–1333.

Mantua, N.J., Hare, S.R., Zhang, Y., Wallace, J.M., Francis, R.C., 1997. A pacific interdecadal climate Oscillation with impacts on Salmon production. Bull. Am. Meteorol. Soc. 78, 1069–1079. https://doi.org/10.1175/1520-0477(1997)078<1069:APICOW>2.0.CO;2.

Mariotti, A., Zeng, N., Lau, K.M., 2002. Euro-Mediterranean rainfall and ENSO-a seasonally varying relationship. Geophys. Res. Lett. 29, 591–594. https://doi.org/10.1029/2001GL014248.

Marj, A.F., Meijerink, A.M.J., 2011. Agricultural drought forecasting using satellite images, climate indices and artificial neural network. Int. J. Remote Sens. 32, 9707–9719. https://doi.org/10.1080/01431161.2011.575896.

Meihan, L., 2022. China's largest freshwater lake sees record early dry season [WWW Document]. In: Sixth Tone. URL. https://www.sixthtone.com/news/1010936/chinas-largest-freshwater-lake-sees-record-early-dry-season-.

Mishra, A.K., Singh, V.P., 2010. A review of drought concepts. J. Hydrol. (Amst.) 391, 202–216. https://doi.org/10.1016/j.jhydrol.2010.07.012.

Mishra, A.K., Singh, V.P., 2011. Drought modeling - a review. J. Hydrol. (Amst.) 403, 157–175. https://doi.org/10.1016/j.jhydrol.2011.03.049.

Moore, G.W.K., Renfrew, I.A., Pickart, R.S., 2013. Multidecadal mobility of the North Atlantic oscillation. J. Clim. 26, 2453–2466. https://doi.org/10.1175/JCLI-D-12-00023.1.

Nguyen, P.L., Min, S.K., Kim, Y.H., 2021. Combined impacts of the El Niño-Southern Oscillation and Pacific Decadal Oscillation on global droughts assessed using the standardized precipitation evapotranspiration index. Int. J. Climatol. 1–18 https://doi.org/10.1002/joc.6796.

Nitta, T., 1987. Convective activities in the tropical western Pacific and their impact on the Northern Hemisphere summer circulation. J. Meteorol. Soc. Jpn. 65, 373–390.

Pegion, K., Kirtman, B.P., Becker, E., Collins, D.C., Lajoie, E., Burgman, R., Bell, R., Delsole, T., Min, D., Zhu, Y., Li, W., Sinsky, E., Guan, H., Gottschalck, J., Joseph Metzger, E., Barton, N.P., Achuthavarier, D., Marshak, J., Koster, R.D., Lin, H., Gagnon, N., Bell, M., Tippett, M.K., Robertson, A.W., Sun, S., Benjamin, S.G., Green, B.W., Bleck, R., Kim, H., 2019. The subseasonal experiment (SUBX). Bull. Am. Meteorol. Soc. 100, 2043–2060. https://doi.org/10.1175/BAMS-D-18-0270.1.

Pieper, P., Düsterhus, A., Baehr, J., 2021. Improving seasonal predictions of meteorological drought by conditioning on ENSO states. Environ. Res. Lett. 16, 094027.

Pillai, P.A., Ramu, D.A., Nair, R.C., 2021. Recent changes in the major modes of Asian summer monsoon rainfall: influence of ENSO-IOD relationship. Theor. Appl. Climatol. 143, 869–881. https://doi.org/10.1007/s00704-020-03454-3.

Robertson, A.W., Vitart, F., Camargo, S.J., 2020. Subseasonal to seasonal prediction of weather to climate with application to tropical cyclones. J. Geophys. Res. Atmos. 125 https://doi.org/10.1029/2018JD029375.

Rodriguez, S., 2022. Seen from space: Extreme drought dries up rivers across the globe. Clim. Home News. https://www.climatechangenews.com/2022/08/26/visuals-extreme-drought-dries-up-rivers-globe-satellite-images/.

Rogers, J., McHugh, M., 2002. On the separability of the North Atlantic oscillation and Arctic oscillation. Clim. Dyn. 19, 599–608. https://doi.org/10.1007/s00382-002-0247-7.

Saji, N.H., Goswami, P.N., Vinayachandran, P.N., Yamagata, T., 1999. A dipole mode in the tropical Indian Ocean. Nature 401, 360–363.

Sehgal, V., Sridhar, V., 2018. Effect of hydroclimatological teleconnections on the watershed-scale drought predictability in the southeastern United States. Int. J. Climatol. 38, 1139–1157. https://doi.org/10.1002/joc.5439.

Shao, J., Wang, J., Lv, S., Bing, J., 2016. Spatial and temporal variability of seasonal precipitation in Poyang Lake basin and possible links with climate indices. Hydrol. Res. 47, 51–68. https://doi.org/10.2166/nh.2016.249.

Shao, W., Chen, X., Zhou, Z., Liu, J., Yan, Z., Chen, S., Wang, J., 2017. Analysis of river runoff in the Poyang Lake Basin of China: long-term changes and influencing factors. Hydrol. Sci. J. 62, 575–587. https://doi.org/10.1080/02626667.2016.1255745.

Shi, P., Yang, T., Xu, C.Y., Yong, B., Shao, Q., Li, Z., Wang, X., Zhou, X., Li, S., 2017. How do the multiple large-scale climate oscillations trigger extreme precipitation? Glob. Planet. Chang. 157, 48–58. https://doi.org/10.1016/j.gloplacha.2017.08.014.

Skea, Jim, Shukla, P.R., Reisinger, A., Slade, R., Pathak, M., Al Khourdajie, A., Diemen, R., 2014. Climate Change 2022 Mitigation of Climate Change - Working Group III Contribution to the Sixth Report of the Intergovernmental Panel on Climate Change. Cambridge University Press.

Sordo, C., Frías, M.D., Herrera, S., Cofiño, A.S., Gutiérrez, J.M., 2008. Interval-based statistical validation of operational seasonal forecasts in Spain condition to El Niño-Southern Oscillation events. J. Geophys. Res. 113, 1–11. https://doi.org/10.1029/2007JD009536.

Stuecker, M.F., Timmermann, A., Jin, F.F., Chikamoto, Y., Zhang, W., Wittenberg, A.T., Widiasih, E., Zhao, S., 2017. Revisiting ENSO/Indian Ocean Dipole phase relationships. Geophys. Res. Lett. 44, 2481–2492. https://doi.org/10.1002/2016GL072308.

Su, H., Neelin, J.D., Meyerson, J.E., 2005. Mechanisms for lagged atmospheric response to ENSO SST forcing. J. Clim. 18, 4195–4215. https://doi.org/10.1175/JCLI3514.1.

Sun, B., Wang, H., 2019. Enhanced connections between summer precipitation over the Three-River-Source region of China and the global climate system. Clim. Dyn. 52, 3471–3488. https://doi.org/10.1007/s00382-018-4326-9.

Sun, H., Hu, H., Wang, Z., Lai, C., 2020. Temporal variability of drought in nine agricultural regions of China and the influence of atmospheric circulation. Atmosphere (Basel) 11. https://doi.org/10.3390/atmos11090990.

Sun, L., Yang, X.Q., Tao, L., Fang, J., Sun, X., 2021. Changing impact of enso events on the following summer rainfall in eastern China since the 1950s. J. Clim. 34, 8105–8123. https://doi.org/10.1175/JCLI-D-21-0018.1.

Sun, B., Wang, H., Li, Huixin, Zhou, B., Duan, M., Li, Hua, 2022. A long-lasting precipitation deficit in South China during Autumn-Winter 2020/2021: combined effect of ENSO and Arctic Sea Ice. J. Geophys. Res. Atmos. 127, 1–18. https://doi.org/10.1029/2021JD035584.

Thompson, D.W.J., Wallace, J.M., 1998. The Arctic oscillation signature in the wintertime geopotential height and temperature fields. Geophys. Res. Lett. 25, 1297–1300. https://doi.org/10.1029/98GL00950.

Thornthwaite, C.W., 1948. An approach toward a rational classification of climate. Geogr. Rev. 38, 55–94. https://doi.org/10.2307/210739.

Tian, B., Fan, K., 2015. A skillful prediction model for winter NAO based on Atlantic Sea Surface Temperature and Eurasian Snow Cover. Weather Forecast. 30, 197–205. https://doi.org/10.1175/WAF-D-14-00100.1.

Toreti, A., Masante, D., Acosta Navarro, J., Bavera, D., Cammalleri, C., De Jager, A., Di Ciollo, C., Hrast Essenfelder, A., Maetens, W., Magni, D., Mazzeschi, M., Spinoni, J., De Felice, M., 2022. Drought in Europe July 2022. Luxembourg. https://doi.org/10.2760/014884, JRC130253.

Torrence, C., Compo, G.P., 1998. A practical guide to wavelet analysis. Bull. Am. Meteorol. Soc. 79, 61–78. https://doi.org/10.1175/1520-0477(1998)079<0061:APGTWA>2.0.CO;2.

Veldkamp, T.I.E., Eisner, S., Wada, Y., Aerts, J.C.J.H., Ward, P.J., 2015. Sensitivity of water scarcity events to ENSO driven climate variability at the global scale. Hydrol. Earth Syst. Sci. Discuss. 12, 5465–5517. https://doi.org/10.5194/hessd-12-5465-2015.

Vicente-Serrano, S.M., Beguería, S., López-Moreno, J.I., 2010. A multiscalar drought index sensitive to global warming: the standardized precipitation evapotranspiration index. J. Clim. 23, 1696–1718. https://doi.org/10.1175/2009JCLI2909.1.

Vicente-Serrano, S.M., López-Moreno, J.I., Gimeno, L., Nieto, R., Morán-Tejeda, E., Lorenzo-Lacruz, J., Beguería, S., Azorin-Molina, C., 2011. A multiscalar global evaluation of the impact of ENSO on droughts. J. Geophys. Res. 116, 1–23. https://doi.org/10.1029/2011JD016039.

Vicente-Serrano, S.M., Beguería, S., Lorenzo-Lacruz, J., Camarero, J.J., López-Moreno, J.I., Azorin-Molina, C., Revuelto, J., Morán-Tejeda, E., Sanchez-Lorenzo, A., 2012. Performance of drought indices for ecological, agricultural, and hydrological applications. Earth Interact. 16, 1–27. https://doi.org/10.1175/2012EI000434.1.

Vicente-Serrano, S.M., McVicar, T.R., Miralles, D.G., Yang, Y., Tomas-Burguera, M., 2020. Unraveling the influence of atmospheric evaporative demand on drought and

its response to climate change. Wiley Interdiscip. Rev. Clim. Chang. 11, 1–31. https://doi.org/10.1002/wcc.632.

Vitart, F., Robertson, A.W., Anderson, D.L.T., 2012. Subseasonal to Seasonal Prediction Project: bridging the gap between weather and climate. WMO Bull. 61, 23–28. https://doi.org/10.1016/C2016-0-01594-2.

Vitart, F., Ardilouze, C., Bonet, A., Brookshaw, A., Chen, M., Codorean, C., Déqué, M., Ferranti, L., Fucile, E., Fuentes, M., Hendon, H., Hodgson, J., Kang, H.S., Kumar, A., Lin, H., Liu, G., Liu, X., Malguzzi, P., Mallas, I., Manoussakis, M., Mastrangelo, D., MacLachlan, C., McLean, P., Minami, A., Mladek, R., Nakazawa, T., Najm, S., Nie, Y., Rixen, M., Robertson, A.W., Ruti, P., Sun, C., Takaya, Y., Tolstykh, M., Venuti, F., Waliser, D., Woolnough, S., Wu, T., Won, D.J., Xiao, H., Zaripov, R., Zhang, L., 2017. The subseasonal to seasonal (S2S) prediction project database. Bull. Am. Meteorol. Soc. 98, 163–173. https://doi.org/10.1175/BAMS-D-16-0017.1.

Wallace, J.M., Gutzler, D.S., 1980. Teleconnection in the geopotential height field during the Northern Hemisphere winter. Mon. Weather Rev. 109, 784–812.

Wang, H., He, S., 2015. The North China/Northeastern Asia severe summer drought in 2014. J. Clim. 28, 6667–6681. https://doi.org/10.1175/JCLI-D-15-0202.1.

Wang, N., Zhang, Y., 2015. Evolution of Eurasian teleconnection pattern and its relationship to climate anomalies in China. Clim. Dyn. 44, 1017–1028. https://doi.org/10.1007/s00382-014-2171-z.

Wang, S., Yuan, X., Li, Y., 2017. Does a strong El Niño imply a higher predictability of extreme drought? Sci. Rep. 7, 1–7. https://doi.org/10.1038/srep40741.

Wang, Z., Yang, S., Lau, N.C., Duan, A., 2018. Teleconnection between summer NAO and East China rainfall variations: a bridge effect of the Tibetan Plateau. J. Clim. 31, 6433–6444. https://doi.org/10.1175/JCLI-D-17-0413.1.

Wang, H., Kumar, A., Murtugudde, R., Narapusetty, B., Seip, K.L., 2019. Covariations between the Indian Ocean dipole and ENSO: a modeling study. Clim. Dyn. 53, 5743–5761. https://doi.org/10.1007/s00382-019-04895-x.

Wang, Yaxu, Lv, J., Hannaford, J., Wang, Y., Sun, H., Barker, L.J., Ma, M., Su, Z., Eastman, M., 2020a. Linking drought indices to impacts to support drought risk assessment in Liaoning province, China. Nat. Hazards Earth Syst. Sci. 20, 889–906. https://doi.org/10.5194/piahs-383-267-2020.

Wang, F., Wang, Z., Yang, H., Di, D., Zhao, Y., Liang, Q., 2020b. Utilizing GRACE-based groundwater drought index for drought characterization and teleconnection factors analysis in the North China Plain. J. Hydrol. (Amst.) 585, 124849. https://doi.org/10.1016/j.jhydrol.2020.124849.

Wei, J., Knoche, H.R., Kunstmann, H., 2015. Contribution of transpiration and evaporation to precipitation: An ET-Tagging study for the Poyang Lake region in Southeast China. J. Geophys. Res. 120, 6845–6864. https://doi.org/10.1002/2014JD022975.

Wei, J., Knoche, H.R., Kunstmann, H., 2016. Atmospheric residence times from transpiration and evaporation to precipitation: An age-weighted regional evaporation tagging approach. J. Geophys. Res. 121, 6841–6862. https://doi.org/10.1002/2015JD024650.

Wei, J., Dong, N., Fersch, B., Arnault, J., Wagner, S., Laux, P., Zhang, Z., Yang, Q., Yang, C., Shang, S., Gao, L., Yu, Z., Kunstmann, H., 2021. Role of reservoir regulation and groundwater feedback in a simulated ground-soil-vegetation continuum: a long-term regional scale analysis. Hydrol. Process. 35, 1–24. https://doi.org/10.1002/hyp.14341.

Wen, N., Liu, Z., Li, L., 2019. Direct ENSO impact on East Asian summer precipitation in the developing summer. Clim. Dyn. 52, 6799–6815. https://doi.org/10.1007/s00382-018-4545-0.

Wood, E.F., Schubert, S.D., Wood, A.W., Peters-Lidard, C.D., Mo, K.C., Mariotti, A., Pulwarty, R.S., 2015. Prospects for advancing drought understanding, monitoring, and prediction. J. Hydrometeorol. 16, 1636–1657. https://doi.org/10.1175/JHM-D-14-0164.1.

Wu, J., Chen, X., 2019. Spatiotemporal trends of dryness / wetness duration and severity : the respective contribution of precipitation and temperature. Atmos. Res. 216, 176–185. https://doi.org/10.1016/j.atmosres.2018.10.005.

Wu, J., Chen, X., Chang, T.J., 2020. Correlations between hydrological drought and climate indices with respect to the impact of a large reservoir. Theor. Appl. Climatol. 139, 727–739. https://doi.org/10.1007/s00704-019-02991-w.

Xiao, M., 2020. Quantifying spatiotemporal influences of climate index on seasonal extreme precipitation based on hierarchical Bayesian method. Int. J. Climatol. 40, 3087–3098. https://doi.org/10.1002/joc.6384.

Xiao, M., Zhang, Q., Singh, V.P., Liu, L., 2016. Transitional properties of droughts and related impacts of climate indices in the Pearl River basin, China. J. Hydrol. (Amst.) 534, 397–406. https://doi.org/10.1016/j.jhydrol.2016.01.012.

Xing, Z., Ma, M., Wei, Y., Zhang, X., Yu, Z., Yi, P., 2020. A new agricultural drought index considering the irrigation water demand and water supply availability. Nat. Hazards 104, 2409–2429. https://doi.org/10.1007/s11069-020-04278-0.

Xing, Z., Yu, Z., Wei, J., Zhang, X., Ma, M., Yi, P., Ju, Q., Wang, J., Laux, P., Kunstmann, H., 2022. Lagged influence of ENSO regimes on droughts over the Poyang Lake basin, China. Atmos. Res. 275, 106218 https://doi.org/10.1016/J.ATMOSRES.2022.106218.

Xu, K., Yang, D., Yang, H., Li, Z., Qin, Y., Shen, Y., 2015. Spatio-temporal variation of drought in China during 1961-2012: a climatic perspective. J. Hydrol. (Amst.) 526, 253–264. https://doi.org/10.1016/j.jhydrol.2014.09.047.

Xu, H., Chen, H., Wang, H., 2021. Interannual variation in summer extreme precipitation over Southwestern China and the possible associated mechanisms. Int. J. Climatol. 41, 3425–3438. https://doi.org/10.1002/joc.7027.

Yang, C., Yu, Z., Hao, Z., Zhang, J., Zhu, J., 2012. Impact of climate change on flood and drought events in Huaihe River Basin, China. Hydrol. Res. 43, 14–22. https://doi.org/10.2166/nh.2011.112.

Yu, M., Li, Q., Hayes, M.J., Svoboda, M.D., Heim, R.R., 2014. Are droughts becoming more frequent or severe in China based on the standardized precipitation evapotranspiration index: 1951-2010? Int. J. Climatol. 34, 545–558. https://doi.org/10.1002/joc.3701.

Yuan, Y., Li, C.Y., 2008. Decadal variability of the IOD-ENSO relationship. Chin. Sci. Bull. 53, 1745–1752. https://doi.org/10.1007/s11434-008-0196-6.

Yuan, C., Zhang, W., Zhong, Y., Lu, X., Liu, J., Wahiduzzaman, M., 2022. North Atlantic forcing of autumn drought in Southwest China. Atmos. Ocean. Sci. Lett. 15, 100152 https://doi.org/10.1016/j.aosl.2022.100152.

Yun, K.S., Seo, K.H., Ha, K.J., 2010. Interdecadal change in the relationship between ENSO and the intraseasonal Oscillation in East Asia. J. Clim. 23, 3599–3612. https://doi.org/10.1175/2010JCLI3431.1.

Zhang, Q., Sun, P., Chen, X., Jiang, T., 2011. Hydrological extremes in the Poyang Lake basin, China: changing properties, causes and impacts. Hydrol. Process. 25, 3121–3130. https://doi.org/10.1002/hyp.8031.

Zhang, Q., Xiao, M., Singh, V.P., Chen, Y.D., 2014. Max-stable based evaluation of impacts of climate indices on extreme precipitation processes across the Poyang Lake basin, China. Glob. Planet. Chang. 122, 271–281. https://doi.org/10.1016/j.gloplacha.2014.09.005.

Zhang, Y., You, Q., Ye, L., Chen, C., 2017. Spatio-temporal characteristics and possible mechanisms of rainy season precipitation in Poyang Lake Basin, China. Clim. Res. 72, 129–140. https://doi.org/10.3354/cr01455.

Zhang, Xu, Dong, Q., Chen, J., 2019a. Comparison of ensemble models for drought prediction based on climate indexes. Stoch. Env. Res. Risk A. 33, 593–606. https://doi.org/10.1007/s00477-019-01650-w.

Zhang, Xuejun, Su, Z., Lv, J., Liu, W., Ma, M., Peng, J., Leng, G., 2019b. A set of satellite-based near real-time meteorological drought monitoring data over China. Remote Sens. 11, 1–12. https://doi.org/10.3390/rs11040453.

Zhang, J., Tourian, M.J., Sneeuw, N., 2020a. Identification of ENSO signature in the boreal hydrological cycle through canonical correlation with sea surface temperature anomalies. Int. J. Climatol. 40, 6219–6241. https://doi.org/10.1002/joc.6573.

Zhang, Q., Yao, Y., Li, Y., Huang, J., Ma, Z., Wang, Z., Wang, S., Wang, Y., Zhang, Y., 2020b. Causes and changes of Drought in China: Research Progress and prospects. J. Meteorol. Res. 34, 460–481. https://doi.org/10.1007/s13351-020-9829-8.

Zhou, L., Wang, S., Du, M., Chen, Q., He, C., Zhang, J., Zhu, Y., Gong, Y., 2021. The influence of ENSO and MJO on drought in different ecological geographic regions in China. Remote Sens. 13, 1–19. https://doi.org/10.3390/rs13050875.

Zhou, B., Qian, J., Zhou, J., Han, T., Sun, B., 2022. Strengthening of the relationship between West China Autumn rain and arctic oscillation in the mid-1980s. Atmos. Res. 265, 105916 https://doi.org/10.1016/j.atmosres.2021.105916.

Zhu, H., He, H., Fan, H., Xu, L., Jiang, J., Jiang, M., Xu, Y., 2020a. Regional characteristics of long-term variability of summer precipitation in the poyang lake basin and possible links with large-scale circulations. Atmosphere (Basel) 11. https://doi.org/10.3390/atmos11101033.

Zhu, X., Hou, C., Xu, K., Liu, Y., 2020b. Establishment of agricultural drought loss models: a comparison of statistical methods. Ecol. Indic. 112, 106084 https://doi.org/10.1016/j.ecolind.2020.106084.

Zscheischler, J., Martius, O., Westra, S., Bevacqua, E., Raymond, C., Horton, R.M., van den Hurk, B., AghaKouchak, A., Jézéquel, A., Mahecha, M.D., Maraun, D., Ramos, A.M., Ridder, N.N., Thiery, W., Vignotto, E., 2020. A typology of compound weather and climate events. Nat. Rev. Earth Environ. 1, 333–347. https://doi.org/10.1038/s43017-020-0060-z.